

This is a preprint of a peer-reviewed article accepted at the journal CLIMATE DYNAMICS. The manuscript posted here is a preprint submitted to EarthArXiv; the final version of this manuscript may change. This pre-print will be updated with the DOI of the final accepted version of this manuscript.

Continental configuration controls the base-state water vapor greenhouse effect: lessons from half-land, half-water planets

Marysa M. Lagu  ^{1,2*}, Gregory R. Quetin³, Sarah Ragen⁴
and William R. Boos^{5,6}

¹Coldwater Lab, Center for Hydrology, University of Saskatchewan, 1151 Sidney Street, Unit 116, Canmore, T1W 3G1, Alberta, Canada.

²Department of Atmospheric Sciences, University of Utah, 135 S 1460 E, ROOM 819, Salt Lake City, 84112-0102, UT, USA
<https://orcid.org/0000-0001-8513-542X>.

³Department of Geography, University of California, Santa Barbara, 1832 Ellison Hall, Santa Barbara, 93106-4060, CA, USA
<https://orcid.org/0000-0002-7884-5332>.

⁴School of Oceanography, University of Washington, 1501 NE Boat St, Seattle, 98195, Washington, USA
<https://orcid.org/0000-0003-0987-6060>.

⁵Department of Earth and Planetary Science, University of California, Berkeley, 307 McCone Hall, Berkeley, 94720-4767, California, USA.

⁶Climate and Ecosystem Sciences Division, Lawrence Berkeley National Lab, 1 Cyclotron Rd, Berkeley, 94720, California, USA
<https://orcid.org/0000-0001-9076-3551>.

*Corresponding author(s). E-mail(s): marysa.lague@utah.edu;

Abstract

The distribution of land and ocean on Earth's surface shapes the global atmospheric circulation and climate by modulating fluxes of water and energy between the surface and the atmosphere. Here we rearranged land in an idealized climate model to explore the effect

2 *Continental configuration controls the base-state water vapor...*

047 of eight simplified continental configurations on global climate, finding
048 several counterintuitive results. The limited capacity of land to hold
049 water and the smaller heat capacity of land compared to ocean—rather
050 than surface albedo differences—are the primary drivers of continental
051 control on global mean temperature. Specifically, the presence of
052 land in certain locations can enhance tropospheric water vapor con-
053 tent, increasing the greenhouse effect and clear-sky shortwave absorption;
054 these effects can warm the planet more than the cooling effect of
055 higher land surface albedos. For example, continental configurations
056 with land in polar regions and large tropical oceans have the warmest,
057 wettest global climates. Configurations with large tropical land masses
058 are not hot desert planets, but have the coolest global climates due
059 to reduced evaporation and thus reduced atmospheric water vapor
060 compared to configurations without land in the tropics. Interactions
061 between the small heat capacity of land and the seasonal cycle can
062 lead to certain continental configurations having even warmer, wet-
063 ter atmospheres than an aquaplanet. Our results demonstrate that
064 different configurations of land, such as those obtained through past tec-
065 tonic movement or on rocky exoplanets, set planetary climate through
mechanisms beyond those involving surface albedo or orographic effects.

066 **Keywords:** Water Vapor, Climate, Continents, Land-atmosphere Interactions

067
068
069
070

1 Introduction

071

072 The distribution of continents on Earth's surface alters both terrestrial and
073 global climate in myriad ways: by modulating surface-atmosphere exchange of
074 water and energy, shaping atmospheric circulation patterns, and delineating
075 ocean basins. Despite its importance, the fundamental role of continental dis-
076 tribution in setting Earth's base-state climate remains poorly understood. In
077 this study, we explore how the distribution of land on Earth's surface alters
078 global evaporation patterns and water vapor concentrations, with implications
079 for global mean surface temperatures and climate.

080 Physical differences between the land and the oceans alter the way the over-
081 lying atmosphere interacts with either surface. The land tends to be brighter,
082 drier, rougher, and have a lower heat capacity than the ocean (Budyko, 1961,
083 1969; Payne, 1972; Bonan, 2008; Jin et al., 2004; Wiscombe and Warren, 1980;
084 Sud et al., 1988; Cess and Goldenberg, 1981; North et al., 1983). Oceans can
085 redistribute energy in the climate system by moving heat laterally while the
086 land cannot (Loft, 1918; Richardson, 1980; Ferrari and Ferreira, 2011). Addi-
087 tionally, while water for evaporation is effectively unlimited in the oceans, the
088 availability of water for evaporation to the atmosphere varies widely over dif-
089 ferent land regions as a function of the local climate (Baldocchi et al., 1997).
090 Terrestrial evaporation and the surface supply of water varies seasonally and
091 behaves differently under different climates. Moreover, while the evaporation
092

from the ocean is governed by atmospheric inputs (i.e. wind speed and radiation), the evaporation from the land surface also varies with soil moisture and physical properties of soil and vegetation that provide resistance to terrestrial evaporation (Manabe, 1969; Bonan, 2008). 093
094
095
096

In slab ocean aquaplanet simulations, the organization of tropical rainfall, the location of the extratropical jet, and the strength of the Hadley circulation are all shown to be impacted by changes in atmospheric water vapor, sea surface temperature, and solar insolation (Kirtman and Shukla, 2000; Barsugli et al, 2005; Kang et al, 2008, 2009; Voigt et al, 2014). The influence of continental configuration on atmospheric water vapor remains largely unexplored; however, recent work has shown that changes in terrestrial evaporation can drastically alter global-scale climate by modifying the total amount of atmospheric water vapor, a strong greenhouse gas (Laguë et al, 2021). In addition, other aquaplanet studies with dynamical oceans illuminate the connection between the distribution of meridional boundaries in the ocean and meridional heat transport, demonstrating how different climates can develop as a result of continental distribution (Enderton and Marshall, 2009; Ferreira et al, 2010). 097
098
099
100
101
102
103
104
105
106
107
108
109

In the modern continental configuration, changes in land surface properties generate large changes in both surface climate and global-scale circulation (Shukla and Mintz, 1982; Charney et al, 1975; Davin et al, 2010; Laguë et al, 2019). Moreover, the complex orography of mountain ranges impacts atmospheric circulation and generates large climate impacts over both land and ocean regions (Queney, 1948; Eliassen and Palm, 1960; Manabe and Terpstra, 1974; Held, 1985; McFarlane, 1987; Held et al, 2002; Maroon et al, 2015; White et al, 2017). While this study focuses on the impact of continental distribution on temperatures, the impact of the location and size of continents on rainfall has been explored extensively in monsoon literature (Dirmeyer, 1998; Yasunari et al, 2006; Maroon and Frierson, 2016; Zhou and Xie, 2018; Hui and Bordoni, 2021). Continental extent also modulates the response of precipitation to reduced terrestrial evaporation (Pietschnig et al, 2021). 110
111
112
113
114
115
116
117
118
119
120
121
122

Idealized modelling studies have further explored how the distribution of land impacts temperature by allowing for albedo feedbacks (Barron et al, 1984) as well as by altering the rate of CO₂ weathering and thus the strength of the CO₂ greenhouse effect (Worsley and Kidder, 1991). Latitudinal variations in albedo are driven directly by land distribution and indirectly through impacts on clouds and sea-ice (Enderton and Marshall, 2009; Voigt et al, 2014). The temperature at each latitude is largely modulated by the meridional heat transport (Pierrehumbert, 2010). Previous theory argues that heat transports by both the atmosphere and ocean, in turn, are largely insensitive to details of the dynamics responsible for the transport of heat, but rather depend more strongly on the mean planetary albedo and the equator to pole albedo gradient (Stone, 1978; Enderton and Marshall, 2009) as well as the evaporation and condensation of water (Fajber and Kushner, 2021). 123
124
125
126
127
128
129
130
131
132
133
134
135
136
137
138

4 *Continental configuration controls the base-state water vapor...*

139 The role of land distribution in modulating global climate has implications
140 for improving our understanding of climate in Earth's geologic past. Recon-
141 structions of Earth's continental configuration over the last several hundred
142 million years span a wide range of continental distributions, sometimes with
143 land clustered into supercontinents, sometimes with land spread widely across
144 the globe as in the modern era (Merdith et al., 2021). Simulations of paleocli-
145 mate include continental configurations vastly different to that of the modern
146 world to study the transition between glacial and interglacial periods (Hoff-
147 man and Schrag, 2002; Hoffman et al., 2017; Voigt et al., 2012), mass extinction
148 events (Penn et al., 2018), and climatic changes due to the opening and closing
149 of oceanic gateways (Straume et al., 2020).

150 We also expect to see different land arrangements on other planets. The
151 habitability of exoplanets is a topic of interest to the astrobiology community
152 (Méndez et al., 2021). The search for planets in the habitable zone hinges on
153 locating the distance from a star that would allow for the presence of liquid
154 water on a planet (a liquid environment is an expected requirement for life
155 and water is the most abundant, common liquid in the universe) (Baross et al.,
156 2007). While it is common to find exoplanets within the habitable zone of a star
157 (Burke et al., 2015), whether or not those planets are actually habitable is dif-
158 ficult to determine (Kite and Ford, 2018). Planets with a vast range of masses,
159 sizes, and orbits have been detected (Seager, 2013), with an anticipated wide
160 range of variability in atmospheric mass and composition; the surface proper-
161 ties of those planets further modulate the planet's habitability (Rushby et al.,
162 2020). The presence of liquid water is often used to determine the habitabil-
163 ity of a planet (Seager, 2013); however, the distribution of hospitable surface
164 climates across a planet will depend on local surface climate.

165 In this study, we explore and compare the climates of eight Earth-like
166 planets, which differ only in their continental configuration. Land differs from
167 ocean in the simulations presented here in three key ways: it has a higher
168 albedo; it has a smaller heat capacity; and it has a limited capacity to hold
169 and evaporate water, with increased resistance to evaporation when the land is
170 not saturated. These differences alter the fluxes of water and energy between
171 the surface and the atmosphere over land vs. ocean, leading to changes in both
172 local surface climate and global-scale climate.

173 We show that the distribution of continents exerts a fundamental control
174 on global climate, even in a model without full representation of the differences
175 between land and ocean. We investigate how the distribution of land and
176 ocean alter planetary surface albedo, total absorbed shortwave radiation at
177 the surface, atmospheric water vapor and the water vapor greenhouse effect,
178 and atmospheric feedbacks resulting from differences in land vs. ocean heat
179 capacity. We conclude with a discussion of the role of land in modulating the
180 base-state climate of a planet, as well as the sensitivity of that climate to
181 changes in terrestrial evaporation.

182

183

184

2 Methods	185
2.1 Model	186
In this study, we use Isca (Vallis et al., 2018), an idealized global circulation model (GCM) to explore the climate of an Earth-like planet with various idealized continental configurations. There is a seasonal cycle in insolation (23.439° obliquity, 0 eccentricity) over a 360-day year. All simulations have atmospheric CO ₂ fixed at 300 ppm. The model is run using a T42 horizontal grid (~2.8°) and 40 vertical levels.	187
The atmosphere uses moist dynamics and produces precipitation, but does not represent the radiative effects of clouds. Therefore, we set the surface albedo of both water and land to a higher value than in a model that represents clouds, allowing for a more reasonable planetary albedo at the top of the atmosphere (see below for more details). In the configuration of the model used here, there are no albedo feedbacks from snow on land or sea ice. The Rapid Radiative Transfer Model (RRTM) (Vallis et al., 2018; Clough et al., 2005; Mlawer et al., 1997) is used for atmospheric radiative transfer, and we use the Simple Betts-Miller convection scheme (Betts, 1986; Betts and Miller, 1986; Frierson, 2007).	188
Analysis is primarily conducted using the Python programming language (Van Rossum and Drake, 2009), particularly with the NumPy (Harris et al., 2020), SciPy (Virtanen et al., 2020), and xarray (Hoyer and Hamman, 2017) packages.	189
2.2 Experiments	190
We run eight simulations, ranging from an all-ocean (Aqua) to an all-land (LandWorld) planet (Fig. 1). For five of the simulations, 50% of the planet's surface is covered by different distributions of land, and ocean covers the remaining 50% of the surface. TropicsLand has a single large continent in a belt around the equator, from 30°S to 30°N, with two oceans over each polar cap. CapLand is the inverse of this, with two continents capping the poles to 30°N/S, and a single large tropical ocean. NorthLand has a single large continent covering the whole northern hemisphere of the planet. EastLand has a single large continent covering the planet from the south to north poles, but only from 0-180°E longitude. In MeshLand, gridcells alternate between land and ocean in a checker-board pattern. Each patch of land/ocean in MeshLand is a single gridcell (roughly 2.8°). All simulations except RealLand have no orography. The RealLand simulation uses a semi-realistic, simplified continental configuration with roughly 20% of the surface covered by land, and idealized orographic representations of the Tibetan Plateau and the Rocky Mountains. This continental configuration is a modified version of that in Saulière et al. (2012), and is produced using Isca's idealized land generator function (Vallis et al., 2018).	191
	192
	193
	194
	195
	196
	197
	198
	199
	200
	201
	202
	203
	204
	205
	206
	207
	208
	209
	210
	211
	212
	213
	214
	215
	216
	217
	218
	219
	220
	221
	222
	223
	224
	225
	226
	227
	228
	229
	230

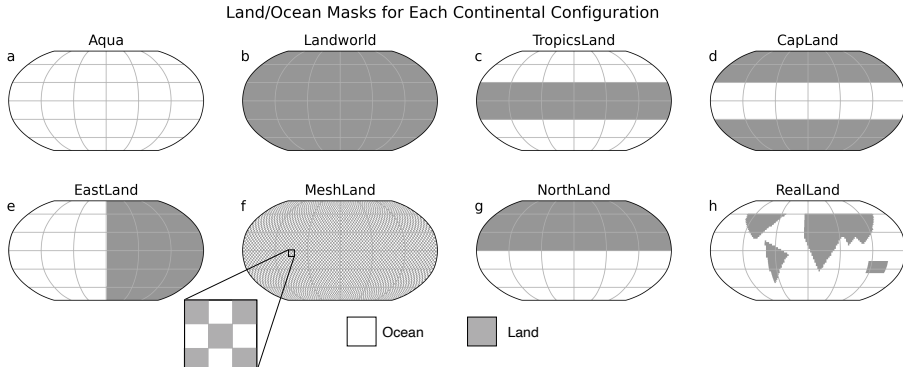
6 *Continental configuration controls the base-state water vapor...*

Fig. 1 Land/ocean masks for each continental configuration. Ocean is shown in white; land is shown in grey. A small section of MeshLand (f) is enlarged to show the land/ocean tiling pattern, where each tile is one gridcell (at roughly 2.8° resolution).

Land differs from ocean in these simulations through its albedo, smaller heat capacity, fixed capacity to hold water, and increased resistance to evaporation under dry soil conditions (table 1). In our simulations, land is 1.3 times brighter than the ocean; the ocean has an albedo of 0.25 and the land an albedo of 0.325. This is brighter than typical albedo values for ocean (Jim et al., 2004) and (snow-free) land (Bonan, 2008), allowing the model to generate similar global mean surface temperatures to our modern climate without the radiative effects of clouds, which increase planetary albedo (Herman et al., 1980).

Table 1 Surface properties of land vs. ocean in all simulations

	Albedo	Capacity hold water [mm]	Heat in equivalent water depth [m]
Ocean	0.25	Unlimited	20
Land	0.325	150 ¹	2

[1] Except in the LandWorld simulation, where water is allowed to accumulate beyond 150 mm.

263
264

265 The land can hold up to 150 mm of water at each point, with soil moisture
266 represented by bucket hydrology. Land is initialized with 100 mm of water
267 at every land gridcell. When the bucket is less than 3/4 full, the evaporative
268 resistance of the land surface increases linearly as a function of soil dryness.
269 When the bucket is more than 3/4 full, the resistance to evaporating water
270 from the land surface is the same as that over open water. Water in excess of the
271 bucket capacity is discarded as runoff; in effect, it is immediately returned to
272 the ocean. However, in LandWorld there is no ocean for runoff to be discarded
273 to, nor is there an oceanic water source to replenish the atmosphere with
274 water; thus, discarding runoff would result in a system that does not conserve
275 water. To address this, hydrology on LandWorld is modified to allow for the
276 formation of lakes: water is allowed to accumulate in excess of the 150mm

bucket capacity, with the evaporative resistance the same as that of open water 277
until the amount of water in the gridcell drops back below 150mm, at which 278
point the standard bucket hydrology rules apply. The atmospheric circulation 279
of LandWorld rapidly transports all of the available moisture to the polar 280
regions where the land forms two “lakes” (see Lagu   et al (2021) for discussion 281
of the formation of polar lakes on an all-land planet). Note that despite the 282
implementation of lakes in the LandWorld simulation, there is still a slow 283
leak of water vapor from the atmosphere which causes the simulation to cool 284
over time (Fig. A1); this is a known bug of Isca that is apparent in all-land 285
configurations (see <https://github.com/ExeClim/Isca/issues/177>) and is not 286
evident in the other simulations which can continuously replenish water vapor 287
from the oceans. 288

The aerodynamic roughness of the land and ocean are the same in these 289
simulations because the effects of surface roughness are outside the focus of 290
this study. In reality, land is typically more aerodynamically rough than the 291
ocean; the implications of this for climate are explored by past studies (Sud 292
et al, 1988; Davin et al, 2010; Lagu   et al, 2019). 293

The ocean is represented with a 20m deep mixed layer ocean that allows 294
sea surface temperatures to evolve. No lateral heat transport is prescribed in 295
these simulations. The heat capacity of the land surface in these simulations 296
is 1/10 that of the ocean, and corresponds to that of a 2m deep mixed layer 297
ocean, a larger value than the heat capacity of typical land surfaces on the 298
modern Earth. The land and ocean heat capacities were selected based on 299
previous Isca simulations that generate realistic climatologies (Thomson and 300
Vallis, 2019; Geen et al, 2018). 301

Simulations are run for 20 years, with the first 4 years discarded to allow 302
for model spin-up. After 4 years, global mean surface temperatures and average 303
terrestrial soil moisture are stable for all simulations except LandWorld, 304
which continues to lose water and cool throughout the length of the simulation 305
(Fig. A1). Over the last decade of the LandWorld simulation, global mean 306
temperatures decrease by roughly 1.5 K, but even without the water leak we 307
expect this simulation to be cold and dry because the atmospheric circulation 308
rapidly transports all the moisture to the polar regions where there is limited 309
energy for evaporation. 310

3 Results & Discussion

3.1 Overview of scenarios

The eight different continental configurations considered here generate a wide 317
variety of climates. The global average annual mean surface temperatures span 318
almost 15 K (Fig. 2), ranging from the coldest global mean surface temperature 319
on LandWorld ($273.0 (\pm 1.2)$ K) to the warmest global mean surface temperature 320
closely shared among RealLand ($286.7 (\pm 0.03)$ K) and CapLand (286.5 321
 (± 0.1) K; numbers in brackets show \pm the interannual standard deviation). 322

8 *Continental configuration controls the base-state water vapor...*

323 **Table 2** Area in millions of km² (global and land-only) with annual mean temperature
 324 above 0°C ($T_{ANN} > 0^\circ\text{C}$), and with annual mean precipitation above 300 mm/year
 325 ($P_{ANN} > 300\text{mm/year}$). Also shown is the % of the total land on each planet meeting
 326 these criteria, and the equator to pole temperature difference in K for each continental
 327 configuration (noted separately for the northern and southern hemispheres for NorthLand
 328 and RealLand, which are not symmetric about the equator).

Continental Configuration	Total Area with $T_{ANN} > 0^\circ\text{C}$, in [km ² × 10 ⁶]	Land Area with $T_{ANN} > 0^\circ\text{C}$, in [km ² × 10 ⁶]	% of Land Area with $T_{ANN} > 0^\circ\text{C}$	Eq to Pole Δ T [K]	Total Area with $P_{ANN} > 300$ [mm/year], in [km ² × 10 ⁶]	Land Area with $P_{ANN} > 300$ [mm/year], in [km ² × 10 ⁶]	% of Land Area with $P_{ANN} > 300$ [mm/year]
Aqua	424	—	—	33	478	—	—
LandWorld	337	337	66	45	57	57	11
TropicsLand	378	260	100	34	273	64	25
CapLand	422	162	65	44	510	250	100
EastLand	396	193	76	43	322	85	33
MeshLand	416	205	80	36	492	244	96
NorthLand	406	188	74	46 (NH), 31 (SH)	432	189	74
RealLand	440	108	91	32 (NH), 29 (SH)	453	81	68

331 Over paleoclimate timescales, global mean temperatures are influenced by
 332 many factors, including changes in atmospheric CO₂ and ocean heat transport
 333 (Tierney et al., 2020). Our results show that continental distribution—
 334 independent of its impacts on CO₂ or ocean circulation—could be a potentially
 335 overlooked contributor to variations in past climate, as the range of surface
 336 temperatures generated solely by altering the continental arrangement and
 337 total amount of land produces changes in global mean surface temperature of
 338 the same order of magnitude as the temperature range experienced on Earth
 339 over the last 500 million years (Voosen, 2019).

340 The spatial distribution of surface temperatures varies between simulations
 341 (Fig. 2). The strongest equator-to-pole annual mean difference in surface tem-
 342 perature occurs over the continent in the NorthLand configuration, followed
 343 by LandWorld and CapLand, while the smallest equator-to-pole temperature
 344 difference occurs in both hemispheres of RealLand, followed by Aqua (Table 2).

345 Along with global temperature, the continental configurations also alter
 346 atmospheric circulation and global mean precipitation, with configurations
 347 with both more and less global mean rainfall than the modern Earth (Fig. 3).
 348 The highest global mean rain value occurs in the CapLand continental configura-
 349 tion (3.27 ± 0.01 mm/day), with the most rain falling over the tropical ocean.
 350 The lowest global mean precipitation values occur in Landworld (0.31 ± 0.16
 351 mm/day).

352 All the continental configurations considered in this study can support
 353 liquid water, a common criteria for planetary habitability (Seager, 2013).
 354 However, the total area of land that would be hospitable to modern terres-
 355 trial ecosystems varies substantially across these continental configurations.
 356 To coarsely quantify the total land area in each simulation hospitable to mod-
 357 ern day terrestrial ecosystems, we calculate the land area in each simulation
 358 with the annual mean temperature above freezing ($T_{ANN} > 0^\circ\text{C}$). We also
 359 calculate the land area with annual mean precipitation above 300 mm/year
 360 ($P_{ANN} > 300\text{mm/year}$), which roughly marks the divide between arid and
 361 semi-arid ecosystems (Salem, 1989).

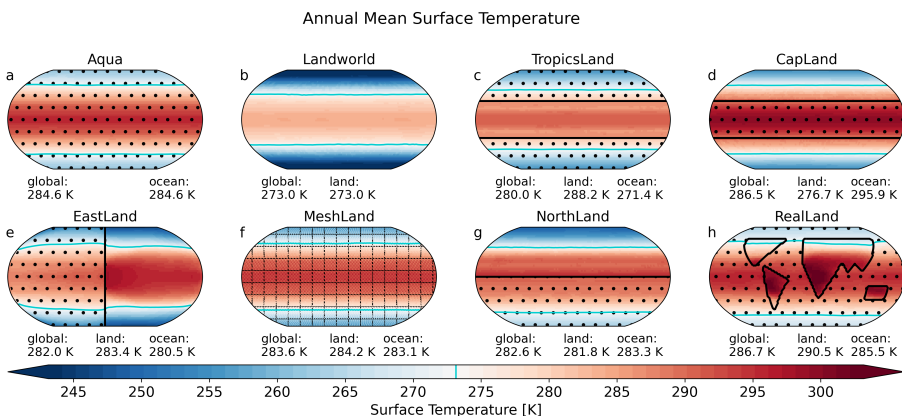


Fig. 2 Maps of annual mean surface temperature [K]. Ocean regions are stippled (except in MeshLand, where diagonal hatching is used to indicate the alternating land/ocean gridcells). Global, land-only, and ocean-only area-weighted annual mean values are noted below each map.

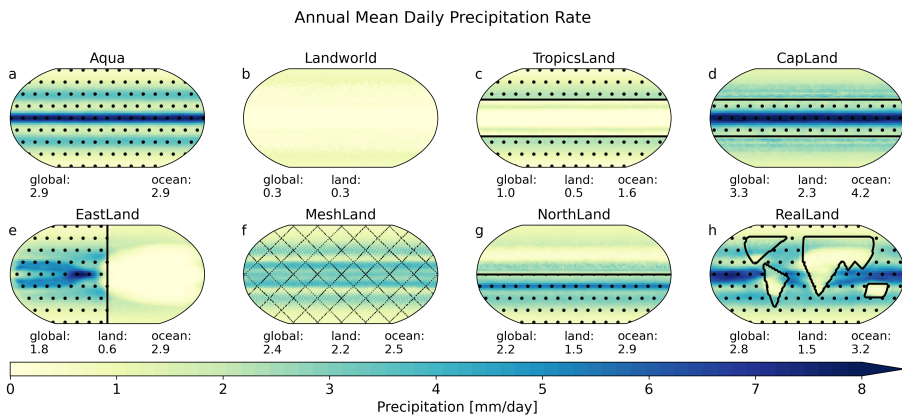


Fig. 3 Maps of annual mean precipitation [mm/day]. Ocean areas stippled (except in MeshLand, where diagonal hatching is used to indicate the alternating land/ocean gridcells). Global, land-only, and ocean-only area-weighted annual mean values are noted below each map.

The spread in the total land area with $T_{ANN} > 0^\circ\text{C}$ across simulations spans hundreds of millions of square kilometers (Table 2). RealLand has the smallest total land with $T_{ANN} > 0^\circ\text{C}$, but it also has the smallest amount of land to begin with. Of the 50/50 land/ocean planets, CapLand and NorthLand have the smallest land area with $T_{ANN} > 0^\circ\text{C}$, while TropicsLand and MeshLand have the most. LandWorld, which has the largest total land area, also has the largest amount of land above freezing in the annual average. However, both LandWorld and TropicsLand have large expanses of very dry land (Table 2). Indeed, only 11% of the land on LandWorld and 25% of the land on TropicsLand have $P_{ANN} > 300\text{mm/year}$. In contrast, 96% and 100% of

10 *Continental configuration controls the base-state water vapor...*

415 the land in MeshLand and CapLand (respectively) exceed the 300 mm/year
 416 precipitation threshold. Climate zone classifications provide a combined esti-
 417 mate of temperature and precipitation impacts on ecosystem distribution;
 418 Köppen-Geiger climate zones for each continental configuration explored here,
 419 calculated following [Kottek et al \(2006\)](#), are shown in Fig. A2.

420 In the sections below, we examine the main drivers of this wide spread
 421 in surface temperatures across the various continental arrangements, with
 422 particular focus on how land distribution impacts surface evaporation and
 423 atmospheric water vapor, the role of albedo, and feedbacks driven by dif-
 424 ferences in land vs. ocean heat capacity. The appendices contain figures
 425 showing transient and seasonal adjustments, meridionally resolved details, and
 426 additional fields of interest.

427

428 3.2 Association of water vapor and the greenhouse effect 429 with surface temperatures

430

431 The various continental configurations explored here have a strong control
 432 on surface evaporation, and thus on the concentration of atmospheric water
 433 vapor. We find that the impact of the continental configuration on water vapor
 434 is the dominant control driving the spread of global mean surface tempera-
 435 tures across simulations, while differences in albedo and absorbed shortwave
 436 radiation play a secondary role.

437 Continental configurations that allow for the largest globally averaged
 438 latent heat flux (evaporation) produce the warmest global mean surface tem-
 439 peratures (Fig. 4a). This contrasts with the intuition of evaporative cooling
 440 leading to cooler surface temperatures. There is a strong linear relationship
 441 ($r^2=0.87$) between the global mean values of surface temperature and sur-
 442 face latent heat flux. Configurations with high surface latent heat flux have
 443 high total column water vapor (Fig. 4b). However, given the temperature-
 444 dependence of water's saturation vapor pressure, we must further explore this
 445 relationship to understand the cause and effect.

446 The total amount and spatial distribution of water vapor, a strong green-
 447 house gas, varies substantially across the continental configurations explored
 448 here (Figs. 4b, 5). All other greenhouse gases are prescribed to be identical
 449 across the simulations. We assess the effect of differences in water vapor con-
 450 centration by approximating the strength of the greenhouse effect (following
 451 [Kiehl and Trenberth \(1997\)](#)) as the difference between longwave (LW) radia-
 452 tion emitted at the surface and emitted at the top of the atmosphere (TOA;
 453 equation 1):

$$454 \quad LW_{diff} = LW_{surface}^\uparrow - LW_{TOA}^\uparrow. \quad (1)$$

455 Small values of LW_{diff} indicate a weak greenhouse effect while large values
 456 indicate a strong greenhouse effect.

457 Across the continental configurations tested, there are a wide variety of cli-
 458 mate states that fall along a common line relating evaporation, water vapor,
 459 and surface temperatures. A strong linear correlation ($r^2 = .82$) exists across
 460 continental configurations between globally averaged latent heat flux and

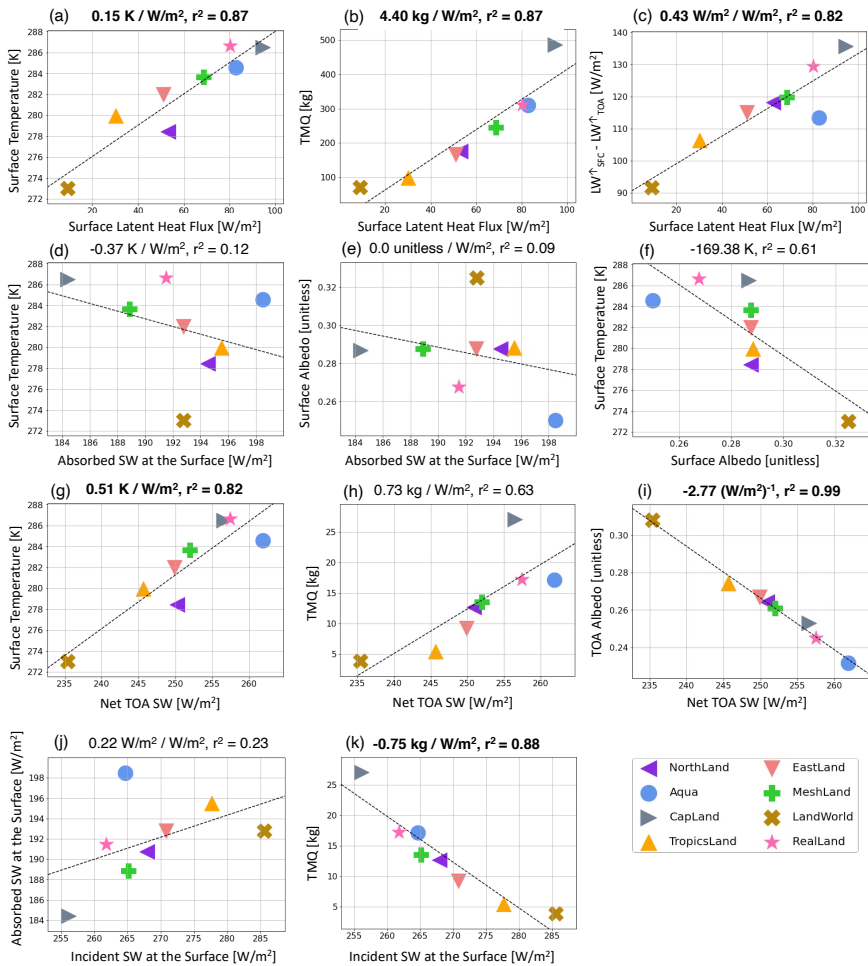


Fig. 4 Scatter plots showing the relationship between various global mean climate variables across the eight continental configurations. All values are shown for the annual mean, with each marker representing an individual continental configuration. The slope and r^2 value of a linear fit (dashed black line) is noted at the top of each panel, with slopes with a p-value < 0.05 shown in bold.

LW_{diff} , where configurations with high surface evaporation—and high water vapor (not shown)—have a stronger greenhouse effect (Fig. 4c). In the following sections, we discuss why each continental configuration leads to each distinct distribution of atmospheric water vapor and surface temperatures.

3.3 Surface albedo differences alone do not explain temperature spread

In our experimental planetary continental configurations, all planets that are 50% land and 50% ocean have the same globally averaged surface albedo. Yet,

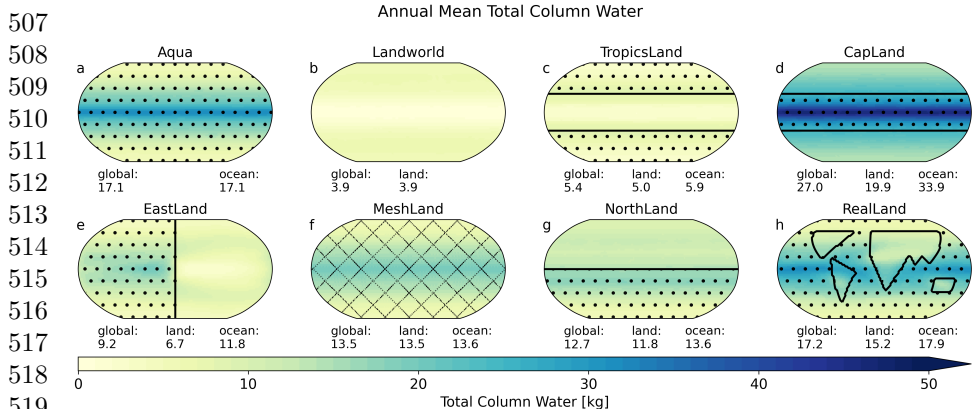
12 *Continental configuration controls the base-state water vapor...*

Fig. 5 Maps of climatological annual mean total atmospheric water vapor [kg] for each continental configuration. Ocean regions are indicated with black stippling, except in MeshLand where gridcells alternate between land and ocean (indicated by checkered hatching, which is not to scale with the model's grid). Global, land-only, and ocean-only area-weighted annual mean values are noted below each map.

for the five continental configurations that are half land and half water and thus with identical surface albedos, there is a roughly 10 K spread in global mean surface temperature (Fig. 4e-g).

Planets with more water (Aqua and RealLand) have an overall darker surface while LandWorld has an overall brighter surface. Surface albedo determines how much of the shortwave radiation energy reaching the surface is absorbed at the planetary surface, and can play a role in controlling surface temperatures by modulating the total amount of energy available to the land surface. Because the model we use does not represent the radiative effects of clouds, we might expect surface albedo to have a stronger impact on top of atmosphere albedo—and thus climate—than in the modern Earth. However, we still see a large spread in the TOA albedo (as shown by the net shortwave radiation flux at the TOA; Fig. 4i), resulting from changes in water vapor.

Along with the surface albedo, the amount of incident shortwave radiation in a region also modulates how much shortwave radiation is available for absorption at the surface. Given the absence of clouds in our simulations, one might hypothesize for simulations with darker ocean near the tropics and brighter land near the poles to absorb more shortwave radiation than simulations with bright land in the tropics since more shortwave radiation is incident at the top of the atmosphere in the tropics than in the high latitudes. However, we find simulations with bright tropical land masses, including TropicsLand and LandWorld, absorb relatively high amounts of shortwave radiation at the surface (Fig. 4d,e). This apparent discrepancy between surface albedo and absorbed shortwave radiation results from more shortwave radiation reaching the surface in configurations with tropical land (Fig. 4h). Water vapor impacts both shortwave and longwave radiative transfer through the atmosphere, and

larger amounts of shortwave radiation reach the surface in TropicsLand and LandWorld because the atmosphere is very dry. 553
554

Top of atmosphere albedo plays a central role in modulating global climate 555
([Donohoe and Battisti, 2011](#)). As our simulations do not have clouds, top of 556
atmosphere albedo is instead a function of surface albedo and water vapor 557
concentrations. The large differences in water vapor across our simulations 558
generate a spread in TOA albedo even among simulations with the same globally 559
averaged surface albedo (Fig. 4f; note that we plot absorbed SW at TOA as 560
a proxy for TOA albedo because all models have identical insolation). There 561
is a correlation ($r^2 = 0.82$) between the globally averaged TOA absorbed SW 562
and global mean surface temperatures, with continental configurations which 563
absorb more net SW radiation at the TOA being generally warmer than 564
configurations which absorb less net SW radiation at the TOA. However, TOA 565
albedo alone does not explain the full spread in surface temperatures across 566
continental configurations. For example, Aqua absorbs the most TOA SW (i.e. 567
has the lowest TOA albedo), but both RealLand and CapLand are warmer. 568

Though the largest difference in surface albedo is between Aqua and Land- 569
World, their difference in globally averaged shortwave radiation absorbed at 570
the surface is fairly small (Fig. 4e). That is, globally averaged surface albedo 571
does not correlate well with globally averaged absorbed surface shortwave radi- 572
ation. While the surface in LandWorld is much more reflective than the surface 573
in Aqua, the dry atmosphere in LandWorld allows a larger amount of solar 574
energy to reach the surface than the moist atmosphere of Aqua (Figs. 4j,k, 575
[5b](#)). Atmospheric water vapor both scatters and absorbs shortwave radiation 576
(even in the absence of clouds), leading to less shortwave radiation incident 577
upon the surface of Aqua than the surface of LandWorld. 578

For the 50/50 land/water planets, which all have the same surface albedo, 579
there is about a 10 W/m² range in total absorbed shortwave radiation (SW) 580
at the surface (Fig. 4e). RealLand, which has a smaller total land area, 581
falls roughly in the middle of the spread. The reason for this non-intuitive 582
relationship between global mean surface albedo and global mean absorbed 583
shortwave radiation at the surface is the result of variations in incident short- 584
wave radiation at the surface between continental configurations, which are 585
due to differences in atmospheric water vapor concentrations. For example, 586
CapLand absorbs a relatively small amount of globally averaged shortwave 587
radiation despite the presence of dark ocean surface in the tropics. However, 588
CapLand has a large concentration of atmospheric water vapor in the tropics 589
(Fig. 5d) due to its tropical ocean. Because atmospheric water vapor scatters 590
and absorbs shortwave radiation, there is less shortwave radiation incident 591
upon the dark tropical surface in CapLand than there is in simulations with 592
drier atmospheres, and thus less shortwave radiation is absorbed despite the 593
dark tropical surface (Fig. 4j). TropicsLand, in comparison, has a much more 594
reflective tropical surface than CapLand, but absorbs more total shortwave 595
radiation because its dry atmosphere allows more solar energy to reach the 596
surface than the humid atmosphere of CapLand. 597

14 *Continental configuration controls the base-state water vapor...*

599 Over sufficiently long timescales, the surface must balance the absorption
 600 of shortwave energy either by heating up (and thus removing energy from
 601 the surface as longwave radiation or sensible heat), or by evaporating water
 602 (removing energy from the surface as latent heat). For land, this occurs on
 603 comparatively short time scales due to its small heat capacity. The larger heat
 604 capacity of the ocean allows it to absorb more shortwave energy before that
 605 energy must be shed as latent heat, sensible heat, or longwave radiation. This
 606 difference in heat capacity plays a critical role in explaining why CapLand is
 607 both warmer and wetter than Aqua, which we discuss in section 3.6. In the
 608 real ocean, heat can also be transported by the ocean circulation, but our
 609 simulations have no ocean circulation by design. The sign of the relationship
 610 between the amount of shortwave radiation absorbed at the surface and the
 611 global mean surface temperature is the opposite of what one might naively
 612 expect: the warmest climates are those that absorb the least amount of SW
 613 radiation at the surface (Fig. 4d). Planets with less land (RealLand, Aqua)
 614 fall above this line, while the planet with more land (LandWorld) falls below
 615 this line.

616 LandWorld is colder than all the other continental configurations despite
 617 the large amount of absorbed SW at the surface (Fig. 4d). CapLand, RealLand,
 618 and Aqua span the full range of simulated globally mean absorbed shortwave
 619 at the surface, yet these three continental configurations are the 3 warmest
 620 planets, with similar global mean surface temperatures (roughly 285 K).

621 This disconnect between globally averaged surface albedo, absorbed SW at
 622 the surface, and surface temperature implies that we cannot rely on the surface
 623 albedo differences of land and water alone to explain the varied climates across
 624 continental configuration. These simulations do not allow for cloud effects on
 625 radiation; however, when cloud impacts on planetary albedo are taken into
 626 consideration for the modern Earth, surface albedo contributes only a small
 627 amount to the top of atmosphere albedo, which controls the total amount of
 628 energy absorbed by the Earth system at any given location (Donohoe et al,
 629 2013).

630

631 **3.4 Longitudinal distribution of land cools by limiting 632 evaporation over the Eastland super-continent**

633 The effect of continental arrangement on surface temperatures and climate
 635 through water vapor vs. albedo is further demonstrated in the comparison of
 636 MeshLand and EastLand. MeshLand and EastLand have the same amount of
 637 land at each latitude. As such, they have the same latitudinal distribution of
 638 surface albedo (or, equivalently, the same insolation-weighted surface albedo).
 639 We find that differences in water vapor driven by differences in evaporation
 640 are the dominant control making MeshLand a warmer planet than EastLand.

641 Despite MeshLand and EastLand having the same latitudinal distribution
 642 of surface albedo, there is more shortwave radiation incident upon the sur-
 643 face in EastLand, so more shortwave radiation is absorbed at the surface of
 644 EastLand compared to Meshland (Fig. 6). If this were the dominant control

on surface climate, we would expect EastLand to be warmer than MeshLand. Instead, we see that MeshLand is warmer; this is a result of differences in the strength of the water vapor greenhouse effect between the two continental configurations.

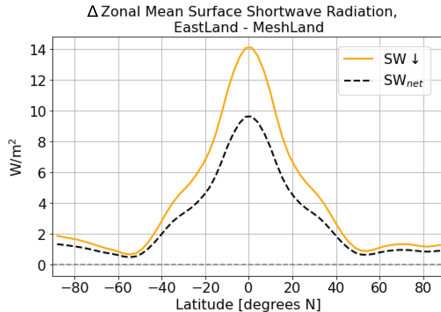


Fig. 6 Zonal mean, annually averaged difference in downwards (yellow) and net absorbed (black) shortwave radiation at the surface for EastLand - MeshLand.

The atmosphere in MeshLand has easy access to water everywhere, as each land gridcell is adjacent to ocean. In contrast, the atmosphere over the continent in EastLand is quite dry (c.f. Fig. 5e,f and A3e,f), particularly in the tropics where moisture that is advected onto the continent quickly precipitates out (Fig. 3e). The humid atmosphere of MeshLand results in a strong water vapor greenhouse effect, which drives the warmer temperatures of MeshLand compared to EastLand. This difference in water vapor also explains the difference in incident shortwave radiation between the two simulations; however, as noted above, this difference in shortwave radiation is not the controlling factor on surface temperature differences between these simulations.

Each MeshLand “island” behaves most similarly to archipelagos like the Maritime Continent, where the surrounding ocean provides moisture and the islands provide vertical motion for rainfall (Kooperman et al., 2017). Meanwhile, the zonal extent of the super continent of EastLand limits the range of moisture transport for precipitation to the interior, similar to Earth’s Asian continent (though more extreme). The resulting dry lands and overlying dry atmosphere of the EastLand super-continent cool the global climate.

In the idealized climate model used in these studies, there are no radiative effects of cloud cover. Cloud radiative effects are an important part of the climate system and can respond strongly to terrestrial processes (Cho et al., 2018; Sikma and Vilà-Guerau de Arellano, 2019; Laguë et al., 2019; Kim et al., 2020), but they also represent a large source of uncertainty (IPCC, 2013; Zelinka et al., 2017). While the radiative effects of clouds would play a role in the climate of all continental configurations considered here, they may be of particular importance in the comparison of MeshLand to EastLand. Specifically, we would expect MeshLand to be cloudy because its atmosphere has ample access to water everywhere and the smaller heat capacity of land would

16 *Continental configuration controls the base-state water vapor...*

691 result in larger sensible heat fluxes over the land than the neighbouring ocean
 692 patches. This combination of vertical motion from sensible heating from the
 693 land and a steady moisture supply from both the ocean and the wet land would
 694 be conducive to the formation of cloud cover along the land/ocean boundary.
 695 The entire planet of MeshLand is comprised of patchy islands—areas which, on
 696 the modern Earth, enhance regional convection, cloud cover, and precipitation
 697 ([Cronin et al., 2015](#)), such as occurs near the Maritime Continent.

698 The patchy nature of MeshLand’s continental distribution, and the resulting
 699 surface heat fluxes, is also reminiscent of regions of patchy deforestation
 700 in the tropics. In the Amazon, deforestation on the scale of tens of km² has
 701 been shown to lead to increased cloud cover at the grass-forest boundary. This
 702 deforestation generates regional circulations driven by sensible heating over
 703 the relatively dry grassland and moisture flux from the relatively moist rain-
 704 forest ([Khanna and Medvige, 2014](#)). Further exploration of a MeshLand-like
 705 planet, potentially with land patches of varying size, in a model that allows
 706 for radiatively interactive cloud cover would be useful to explore the impact
 707 of coastal land on cloud formation at different latitudes.

708 Another process that strongly impacts cloud formation and precipitation
 709 over complex topography is orographic lift ([Kirshbaum and Smith, 2009](#);
 710 [Houze, 2012](#); [Maroon et al., 2015](#)). Elevated orography can drive circulations
 711 and alter free-tropospheric temperature and regional climate, but the physics
 712 of this are complex and interact strongly with surface albedo ([Hu and Boos,](#)
 713 [2017](#)). With the exception of RealLand, which has a simplistic representation
 714 of some mountain ranges, orographic effects are not represented in these flat-
 715 land simulations. Rather than exploring the orographic effects of continents
 716 on climate, here we are specifically focused on the differences in land vs. ocean
 717 heat capacity, albedo, and evaporative properties and their effect on climate.
 718

719 **3.5 Large tropical landmasses limit atmospheric water 720 vapor**

721 The coldest three simulations (LandWorld, Northland, and TropicsLand) all
 722 have relatively large amounts of tropical land cover. These simulations are
 723 colder than the others at most latitudes in the annual mean (Fig. 2 and [A4](#)).
 724 Even EastLand, in which half of the tropics are covered by land, is cooler and
 725 drier than the simulations with open water across the entire tropics. Land can
 726 affect the global water vapor concentration both through evaporation and by
 727 changing the saturation vapor pressure of the atmosphere through changes in
 728 air temperatures.

729 Albedo differences between land and ocean cannot explain why configura-
 730 tions with large tropical land masses are cooler than other configurations. As
 731 discussed in section [3.3](#), the total amount of shortwave radiation absorbed at
 732 the surface is similar between these three simulations, and is higher than any
 733 other planet except Aqua (Fig. 4). Low shortwave radiation absorption over
 734 the tropical continents doesn’t explain the cooler global temperatures—thus
 735 we examine differences in evaporation between simulations.

Generally, land is a dryer surface with limited water holding capacity compared to the ocean, and so serves to limit evaporation over the continents. The evaporative demand of the atmosphere is high in the tropics because of the warmer tropospheric air driven by high insolation. When there is ocean in the tropics, this evaporative demand is supplied by an effectively infinite reservoir of surface water. However, when the tropics are covered with land, the water on the land is quickly evaporated. While some of this moisture initially rains onto the land surface, e.g. in a classic intertropical convergence zone that occupies a narrow range of latitudes, tropical moisture export events (e.g. see Knippertz and Wernli, 2010) move moisture off the tropical continent. Eventually the tropical land dries out except along the edges of the continent, which experience seasonal precipitation.

The large latitudinal extent of the continent (between 30 degrees N-S) inhibits near-surface atmospheric moisture transport into the continental interior from the polar oceans. That is, were the equatorial continent of a smaller latitudinal extent, the equatorward component of the trade winds would travel over ocean (evaporating water along the way) before making landfall, thus bringing moisture onto the continent. With a latitudinally wide tropical continent, the near-surface winds travelling equatorward lie over land, thus the air is much drier than if the wind was travelling over an ocean surface. This results in most of the TropicsLand continent being dry, which means the tropical atmosphere cannot evaporate a large amount of moisture from the surface, resulting in a dry tropical atmosphere (Fig. A5).

In the modern continental configuration, near-surface winds in the tropics move moisture equatorward. However, in TropicsLand, the subsiding branch of the Hadley cell doesn't extend beyond the polar edge of the continent except in local summer. A small amount of moisture is brought onto the continental edge in summer (Fig. A5), but for the most part, surface winds in the low latitudes in TropicsLand do not travel over the ocean surface and thus do not transport moisture equatorward. In equilibrium, the large tropical land masses considered in this study are very dry and serve as a cap to tropical evaporation (Fig. 7).

Limited evaporation also means less latent cooling of the land surface, which could warm these tropical continents. However, the reduction of the water vapor greenhouse effect causes the continents to stay cool year round. The atmosphere at all latitudes becomes depleted in atmospheric water vapor (Fig. 5, A3). Instead of the surface temperature rising without evaporation, the atmosphere, robbed of its main source of moisture by the land surface, dries out and drives surface cooling via a reduced greenhouse effect. The weak greenhouse effect from low atmospheric water vapor is evident in the smaller magnitude of downwelling LW radiation at the surface in TropicsLand, LandWorld, and over the continent in Northland (Fig. A6). The water vapor feedback that operates in response to an arbitrary radiative forcing is expected to further reduce surface temperatures, amplifying the cooling produced by the initial land-induced drying.

737
738
739
740
741
742
743
744
745
746
747
748
749
750
751
752
753
754
755
756
757
758
759
760
761
762
763
764
765
766
767
768
769
770
771
772
773
774
775
776
777
778
779
780
781
782

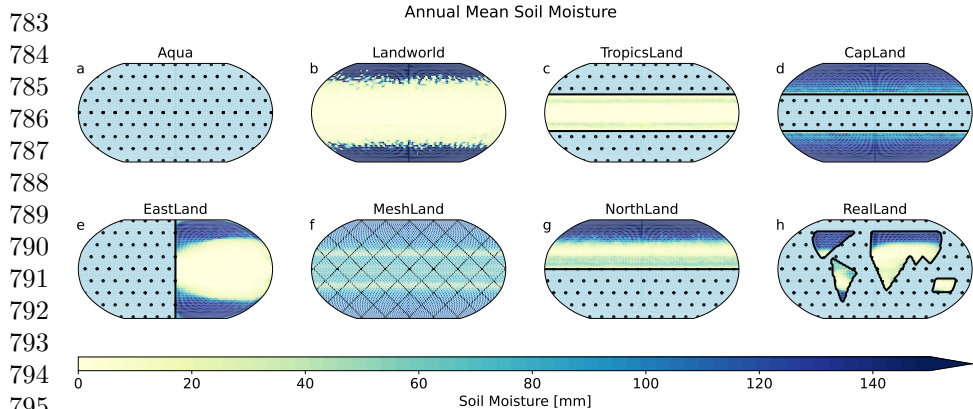
18 *Continental configuration controls the base-state water vapor...*

Fig. 7 Maps of annual mean soil moisture [mm]. Ocean areas are shown in light blue with stippling (except in MeshLand, where diagonal hatching instead of stippling indicates the alternating land/ocean gridcells). Note that all land regions have a maximum water-holding capacity of 150 mm except LandWorld, which has been modified to allow for lake formation to conserve water.

While there is ample water available for evaporation at higher latitudes—e.g. over the polar oceans in TropicsLand, from high-latitude soil moisture in NorthLand and Landworld, or from the southern hemisphere ocean in NorthLand—the lack of energy for evaporation at higher latitudes and horizontal mixing by the atmospheric circulation together maintain a dry tropical atmosphere in these simulations. The mid-to-high latitude atmosphere in TropicsLand does not contain nearly as much water vapor as the Aqua, CapLand, MeshLand, or RealLand continental configurations (Figs. 5 and A3). The southern hemisphere in NorthLand has much more water vapor than the northern hemisphere, which is consistent with the warmer surface temperatures of the southern hemisphere. The tradeoff between surface warming from reduced evaporation and large-scale surface cooling from a reduced atmospheric water vapor greenhouse effect is explored in detail for Northland in Lagu   et al (2021).

The colder climates seen in our simulations with extensive tropical land cover may resemble Snowball Earth conditions, when tropical oceans were hidden beneath sea glaciers (Hoffman et al, 1998), or during past geological epochs when land was clustered into large tropical supercontinents (Chandler et al, 1992; Merdith et al, 2021). Though not explored here, we note that differences in ocean dynamics on paleoclimate timescales can also be large drivers of differences in climate even with approximately similar continental configurations (Chiang, 2009).

In addition to their dry atmospheres, the atmospheric circulations of LandWorld, TropicsLand, and NorthLand differ drastically from those of the other continental configurations. The meridional streamfunctions of the other continental configurations qualitatively resemble those of the modern Earth (Fig. 8).

However, for LandWorld, TropicsLand, and NorthLand, the dry tropical land-masses are highly depleted of soil moisture, and as such the tropical Hadley circulation is not dominated by moist dynamics, but rather by dry convection. The result is an overturning circulation which is vertically very short, and resembles the Hadley circulation expected for Snowball Earth (Voigt et al., 2012; Voigt, 2013) or the shallow meridional circulations over deserts (Zhai and Boos, 2017). In the case of NorthLand, this only applies to the northern hemisphere.

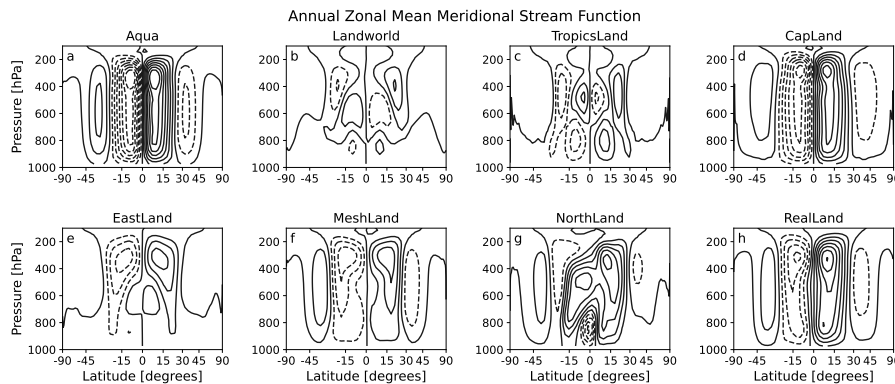


Fig. 8 Zonal mean meridional stream function (annually averaged) for each continental configuration. Contours are spaced at 0.2×10^{11} kg/s. Solid contours indicate positive values (clockwise flow in this view) while dashed contours indicated negative values (counterclockwise flow).

3.6 Land heat capacity drives a seasonally asymmetric feedback with evaporation and water vapor

In this section, we focus on the differences between CapLand and Aqua, to explain why a planet that is 50% land covered is warmer and has more atmospheric water vapor than an aquaplanet where the entire planetary surface is ocean. The open tropical oceans in Aqua and CapLand result in these two simulations experiencing the most total evaporation and atmospheric water vapor of all our simulations (Figs. 4, 5). Note that in terms of global mean surface temperature, these simulations are the closest analogs to RealLand, which also has high surface evaporation and total atmospheric water vapor compared to other continental configurations.

The dark tropical ocean surface with effectively unlimited water for evaporation results in a moist tropical atmosphere for both CapLand and Aqua. Initially, water evaporated over the lower latitude ocean falls as precipitation on the equatorial edge of the polar continents of CapLand before it is evaporated again and transported by transient eddies to higher latitudes. Atmospheric moisture transport in CapLand provides enough water to maintain high soil moisture all year long (Figs. 7 and A7). We note, however, that

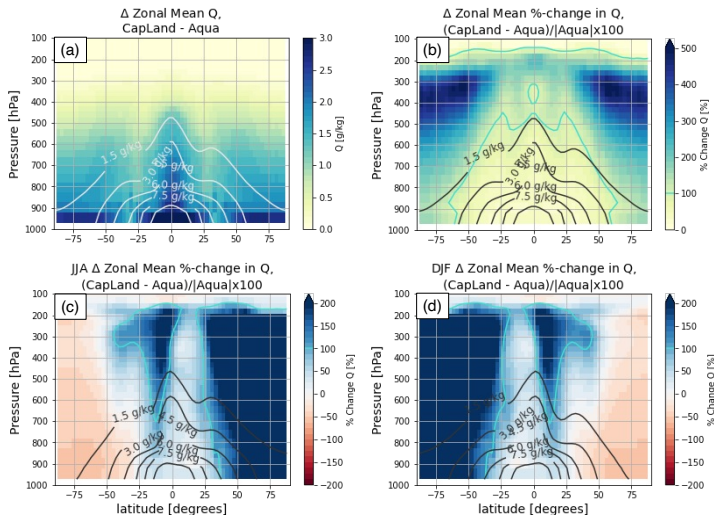


Fig. 9 Difference (CapLand – Aqua) in zonally averaged (a) annual mean specific humidity [g/kg] is shown in shading, with the climatological specific humidity [g/kg] from Aqua show in white contours. (b–c) show the percent change specific humidity for (b) the annual mean, (c) DJF, and (d) JJA in shading, with black contours showing climatological specific humidity [g/kg] from Aqua. Cyan contours in (b–d) show the 100% change in specific humidity line.

both CapLand and Aqua experience temperatures below freezing at the high latitudes during winter (Fig. A4), and thus we would expect the surface to be frozen for part of the year—but these simplified simulations do not account for the effects of sea ice or snow.

Despite its greater amount of land surface, CapLand is both warmer and has more atmospheric water vapor at all latitudes than Aqua (Fig. 9). This is particularly evident in the higher latitudes at higher levels of the troposphere, where the atmosphere in CapLand has over 100%—and in places in excess of 500%—more water vapor (in terms of specific humidity) than Aqua. While high soil moisture on the CapLand continents allows the surface to supply water to the atmosphere, the CapLand continent still differs from the high latitude ocean in Aqua in that it is brighter (higher albedo) and has a lower heat capacity.

The difference in both mean annual temperature and water vapor can be explained by the increased variation of seasonal temperature due to the land’s lower heat capacity and a seasonal feedback through water vapor. Over land, the smaller heat capacity results in a larger seasonal amplitude of temperature than over ocean. CapLand has seasonally warmer local summers and cooler winters over the polar continent than over the oceans at the same latitude in Aqua (Fig. 10c,d). This increase in amplitude is expected; however, an increase in the annual mean temperature is not.

To explain the observed increase in mean temperature, we must consider two factors: (i) energy can be shed from the land surface not only as long-wave radiation (LW), but also as sensible heat (SH) or evaporation/latent heat

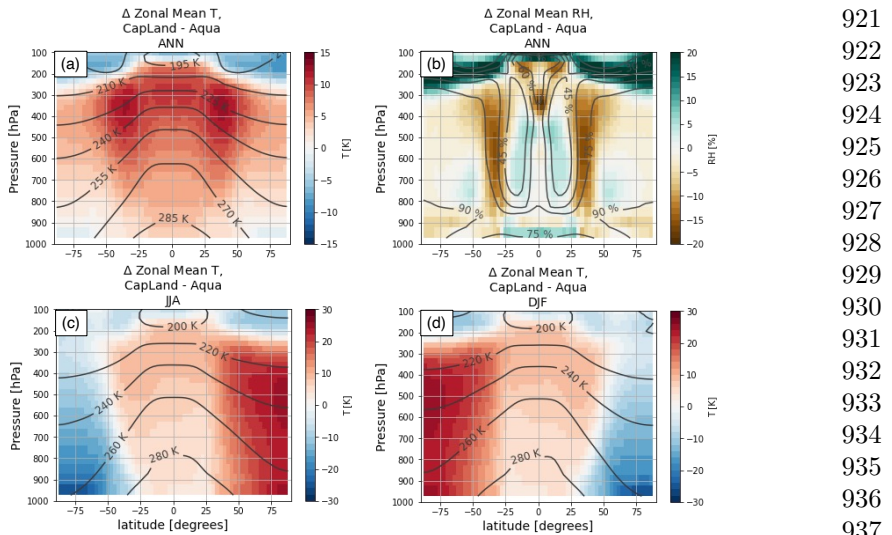


Fig. 10 Difference (CapLand – Aqua) in zonally averaged (a) annual mean air temperatures, (b) annual mean relative humidity, (c) DJF air temperatures and (d) JJA air temperatures, from the surface to 100 hPa. Contours show the climatological values for each field from the Aqua simulation.

(LH), and (ii) feedbacks due to water vapor through the greenhouse effect and atmospheric energy transport. The seasonal imbalance between the local winter and summer is a result of a feedback between surface evaporation and the water vapor greenhouse effect.

During local summer, there is an increase in the total amount of radiative energy flowing into the land surface ($SW + LW$) in CapLand (Fig. 11a-c). This energy is shed from the land surface through a combination of increased surface temperatures (as evident by increased LW^\downarrow and SH), and increased surface evaporation (Fig. 11d-f). This leads to more atmospheric water vapor; because of the non-linearity of the Clausius Clapeyron relationship, the summer increase in specific humidity has a larger magnitude than the winter decrease (Fig. 9). Due to the increase in atmospheric water vapor during local summer, less incoming shortwave radiation reaches the surface (Fig. 11b). However, the increase in LW^\downarrow into the surface is much larger than this decrease in SW^\downarrow (Fig. 11a-c). The increase in LW^\downarrow is a result of higher atmospheric temperatures and increased atmospheric water vapor, leading to a stronger greenhouse effect (which also helps to increase atmospheric temperatures).

Increased LW^\downarrow into the surface adds energy into the land system, increasing the energy available for evaporation from the land. In CapLand, the soils remain wet through the summer (because of atmospheric moisture transport onto the continent; Figs. 7 and A7), supplying water to the hotter atmosphere and completing the feedback loop.

This evaporation-water vapor-greenhouse feedback is only possible because the continent in CapLand is very moist. Without available water on the polar

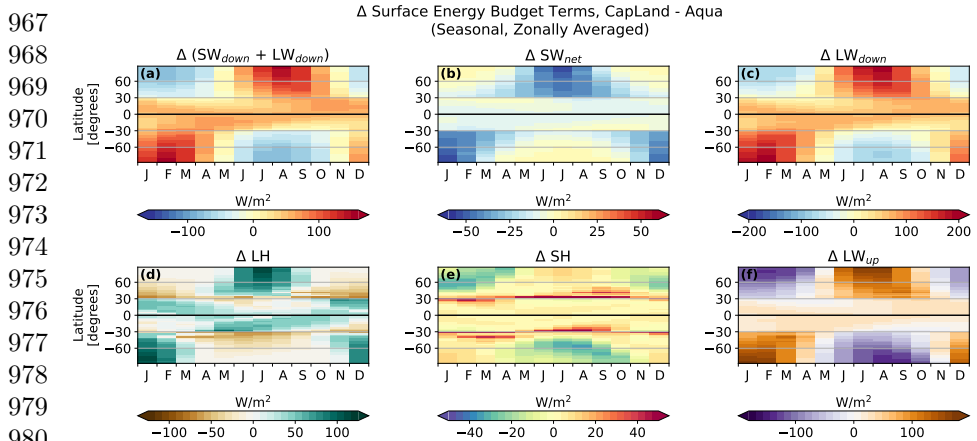


Fig. 11 Hovmoller plots showing the seasonal cycle of the difference in zonally averaged surface energy fluxes between CapLand and Aqua. The total radiative energy flux into the surface is shown in (a), separated into the net absorbed SW in (b) and the downwelling LW in (c). Panels d-f show the fluxes of energy leaving the surface, as latent heat flux (evaporation) in (d), sensible heat flux in (e), and emitted longwave radiation in (f). Note the difference in the scale of the color bars between panels.

continents, the small heat capacity of land would lead to warming but no change in evaporation rates in summer. In this hypothetical dry polar land scenario, the water vapor–greenhouse feedback would be much weaker or would not occur at all. The moist polar continents buffer the summer surface temperature response as excess energy from the strengthened greenhouse effect goes into evaporating more water rather than into warming the surface, which further strengthens the greenhouse effect. There is very little change in sensible heat flux at the surface between CapLand and Aqua, except right along the continental boundary (Fig. 11e).

The increased energy into the surface, increased evaporation, stronger water vapor greenhouse effect, and the resulting increase in energy into the surface are specific to summer, and create a seasonal imbalance in atmospheric air temperatures and atmospheric water vapor between summer and winter on CapLand vs. Aqua. The atmosphere over the continent in CapLand during local winter is slightly drier than the atmosphere over Aqua's ocean at the same latitude. In contrast, during local summer the atmosphere over CapLand is much more humid than the atmosphere over Aqua's ocean at the same latitude (Fig. 10). Concurrently, the magnitude of warming in summer is larger throughout the atmospheric column than the magnitude of cooling in winter. Only at low altitudes above the land surface is the winter cooling comparable to the summer warming in CapLand vs. Aqua (Figs. 10, 11f). The small heat capacity of land interacting with the seasonal cycle drives this feedback, which is why summer temperatures are amplified in CapLand vs. in Aqua. This summertime CapLand-specific feedback does not occur in winter because evaporation is low in both CapLand and Aqua.

The non-linear relationship between longwave radiation and surface temperature could also introduce seasonally asymmetric temperature responses, however in our simulations, this relationship fails to explain our results. If we were to assume that the difference in insolation between summer and winter must be removed from the land surface as longwave radiation through a change in surface temperature (i.e. ignoring sensible or latent heat flux) and that the change in insolation is equal and opposite in summer vs. winter, then by the Stefan–Boltzmann law ($LW \propto \sigma T^4$ (Stefan, 1879)), a *larger* change in surface temperature is needed during the cold season than is needed during the warm season in order to produce the same anomalous magnitude of longwave radiation. However, we do not find this in our simulations (Fig. 10c/d). Moreover, the critical difference in the CapLand vs. Aqua climate at high latitudes is the amplified amount of energy into the CapLand surface during local summer.

Past studies have explored similar idealized continental configurations to CapLand and TropicsLand, with opposing conclusions on which configuration makes for the warmer planet. Worsley and Kidder (1991) found that the tropical continental configuration allows for greater removal of CO₂ from the atmosphere through weathering and thus results in a cooler climate due to a diminished greenhouse effect. In contrast, Barron et al (1984) found the polar continental configuration generates the cooler climate as it provides a surface for high-latitude snow accumulation, which generates cooling through snow albedo feedbacks. In this study, we identify a third mechanism of importance: a planet with moist land capping the poles and a tropical ocean is warmer than the planet with a tropical land belt and polar oceans because the continental arrangement exerts strong controls on evaporation and atmospheric water vapor.

A critical difference between our simulations and those of Barron et al (1984) and Worsley and Kidder (1991) is our inclusion of a seasonal cycle. Without seasonality, the low heat capacity of land and the resulting summertime evaporation-water vapor-greenhouse effect feedback does not occur; this summertime warming feedback is the primary driver for our warmer CapLand simulation compared to Aqua. Moreover, our simulations do not allow for changing albedo from clouds, snow, or sea ice, nor changes in CO₂ due to weathering. Macdonald et al (2019) find arc-continent collisions in the low latitudes increase the removal of atmospheric CO₂ through intensified chemical weathering, a similar mechanism to that invoked by Worsley and Kidder (1991). However, the weathering mechanism requires the tropical continent to receive adequate moisture to allow for rock weathering. Yet our TropicsLand simulation provides a potential counterexample to this, where a large tropical land mass could have low weathering rates due to the dry atmosphere with limited precipitation. While we do not simulate rock weathering impacts on atmospheric CO₂ in our simulations, we would expect weathering rates to be lower over TropicsLand than, for example, MeshLand, which has much higher precipitation rates over land. That is, the intensity of weathering in the low

1013
1014
1015
1016
1017
1018
1019
1020
1021
1022
1023
1024
1025
1026
1027
1028
1029
1030
1031
1032
1033
1034
1035
1036
1037
1038
1039
1040
1041
1042
1043
1044
1045
1046
1047
1048
1049
1050
1051
1052
1053
1054
1055
1056
1057
1058

1059 latitudes requires not only the presence of land, but also the presence of pre-
 1060 cipitation. However, if our tropical continent were smaller in extent, allowing
 1061 for more atmospheric water vapor and precipitation, the potential for CO₂
 1062 removal from rock weathering would likely be higher.

1063

1064

1065 4 Conclusions

1066

1067 The distribution of land exerts a first-order control on global climate by
 1068 modulating atmospheric water vapor concentrations. The eight idealized con-
 1069 tinental configurations considered here produced climates that span a range of
 1070 roughly 15 K in global mean surface temperatures. We find strong relationships
 1071 between surface evaporation, surface temperatures, and total atmospheric
 1072 water vapor across the simulations.

1073 While the climate of each continental configuration considered here differs,
 1074 the mechanisms controlling these climates share many commonalities; in par-
 1075 ticular, each includes a feedback with the greenhouse effect of water vapor.

1076 When large landmasses are positioned in high insolation areas like the tropics,
 1077 as is the case with TropicsLand, LandWorld, NorthLand, and EastLand, we do
 1078 not get hot desert worlds; instead, the relatively dry land leads to water vapor
 1079 depletion and a relatively cool climate. Our modern continental configuration
 1080 drives a climate that is among the warmest and wettest of the configurations
 1081 explored here, which is consistent with our findings that continental configu-
 1082 rations with large tropical ocean area have warm, moist atmospheres. While
 1083 there is land at low latitudes on modern Earth, there is also extensive ocean
 1084 area; the relatively wet atmosphere of RealLand suggests that the modern
 1085 Earth continental configuration does not limit tropical evaporation or tropical
 1086 atmospheric water vapor.

1087 Also of great importance is the fact that the low heat capacity of a wet
 1088 continent at the poles in CapLand creates a larger seasonal cycle of tempera-
 1089 ture and generates a seasonal evaporation/water vapor feedback that amplifies
 1090 summer warming. This feedback creates a climate that is wetter and warmer
 1091 on a planet with 50% land cover than on an aquaplanet without continents.

1092 Our framework allows us to isolate a new mechanism through which trop-
 1093 ical vs. extratropical land masses can modulate global-scale climate, and
 1094 also highlights the importance of continental distribution for global climate
 1095 through its influence on atmospheric water vapor. Further study is required
 1096 to determine the combined climate effects of tropical vs. extratropical land
 1097 on long-term atmospheric CO₂ concentrations, surface albedo (through snow
 1098 cover), and top-of-atmosphere albedo (through cloud cover and water vapor
 1099 effects). How much these various effects may amplify, damp, or generate
 1100 interactions which could further feed back on global climate is necessary to
 1101 understand the total impact of continental distribution on global-scale climate.

1102 The different continental configurations explored here are idealizations, but
 1103 provide possible analogues for past continental configurations (see [Meredith
 1104 et al \(2021\)](#)), or configurations on different water-land planets. We show how

the distribution of land on a planet's surface has a fundamental control on	1105
surface climate by modulating atmospheric water vapor concentrations and	1106
creating feedbacks between heat capacity and the seasonal cycle, with varia-	1107
tions in the distribution of a fixed amount of land across the planetary surface	1108
generating a substantial spread in global mean surface climate.	1109
	1110
	1111
	1112
	1113
	1114
	1115
	1116
	1117
	1118
	1119
	1120
	1121
	1122
	1123
	1124
	1125
	1126
	1127
	1128
	1129
	1130
	1131
	1132
	1133
	1134
	1135
	1136
	1137
	1138
	1139
Acknowledgments. This research used the Savio computational cluster	1140
resource provided by the Berkeley Research Computing program at the Uni-	1141
versity of California, Berkeley (supported by the UC Berkeley Chancellor,	1142
Vice Chancellor for Research, and Chief Information Officer). This research	1143
used resources of the National Energy Research Scientific Computing Center	1144
(NERSC), a U.S. Department of Energy Office of Science User Facility located	1145
at Lawrence Berkeley National Laboratory, operated under Contract No. DE-	1146
AC02-05CH11231. We acknowledge high-performance computing support for	1147
analysis using the Casper platform of Cheyenne (doi:10.5065/D6RX99HX)	1148
provided by NCAR's Computational and Information Systems Laboratory,	1149
sponsored by the National Science Foundation.	1150

Appendix A Spinup & Additional Fields of Interest

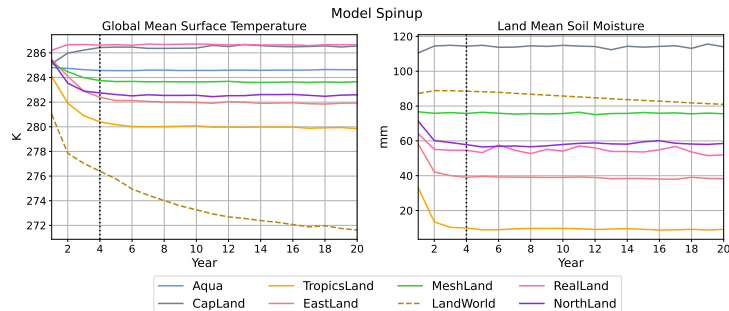


Fig. A1 Annual mean (a) global-mean surface temperature [K] and (b) land-mean soil moisture (water in soil “bucket”, in [mm]) for each model simulation, showing equilibration within 4 years of initialization for all simulations except LandWorld (dashed tan line). The vertical dotted at year 4 marks the end of the spin-up period; model output up to and including year 4 are discarded from the analysis in this study.

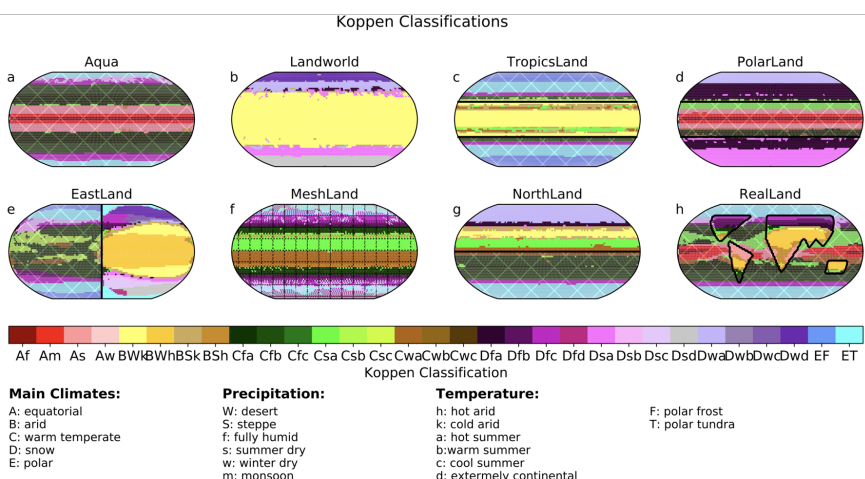


Fig. A2 Köppen-Geiger climate zones for each continental configuration, calculated following Köttek et al (2006).

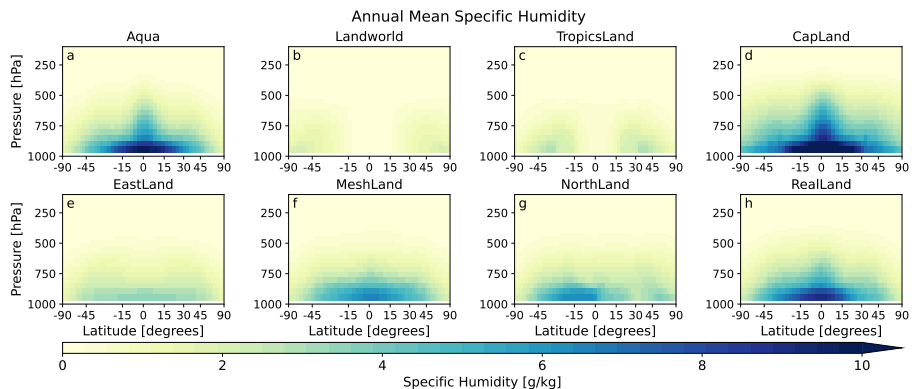


Fig. A3 Zonally averaged annual mean specific humidity from the surface to 100 hPa for each continental configuration.

Appendix B Transient and seasonal adjustments

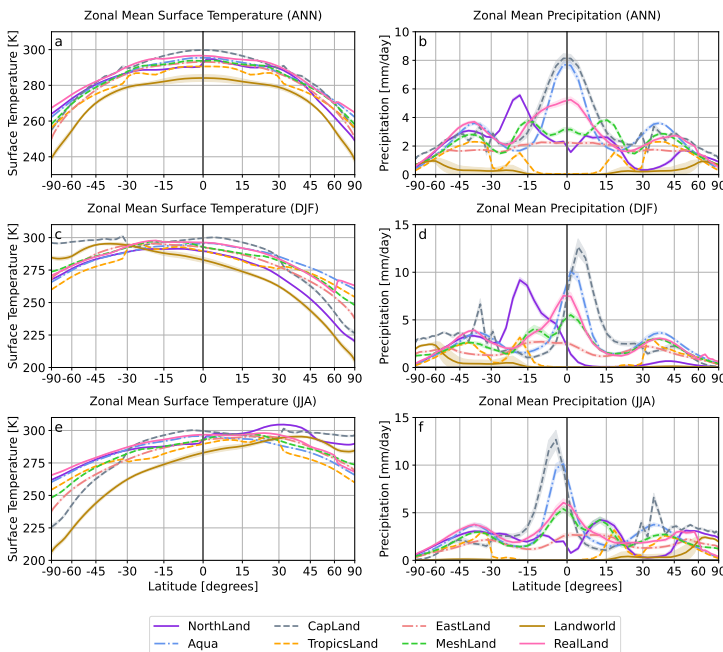
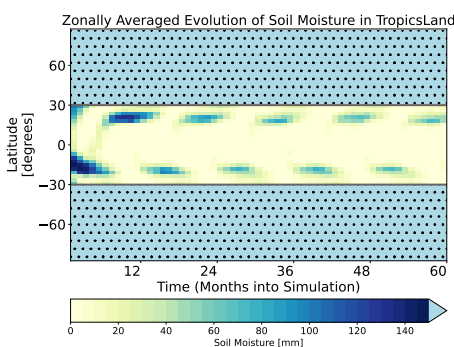


Fig. A4 Zonally averaged surface temperature (left) and precipitation (right) for each simulation in the annual mean (top), DJF (middle) and JJA (bottom).

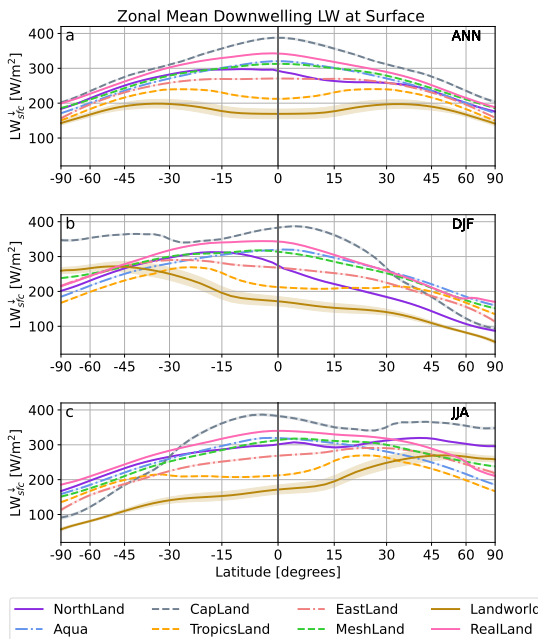
1197
1198
1199
1200
1201
1202
1203
1204
1205
1206
1207
1208
1209
1210
1211
1212
1213
1214
1215
1216
1217
1218
1219
1220
1221
1222
1223
1224
1225
1226
1227
1228
1229
1230
1231
1232
1233
1234
1235
1236
1237
1238
1239
1240
1241
1242

1243
1244
1245
1246
1247
1248
1249
1250
1251
1252
1253
1254
1255



1256 **Fig. A5** Hovmoller plot showing the evolution of zonally averaged soil moisture for the
1257 first five years of the TropicsLand simulation [mm]. Ocean areas are indicated by light blue
1258 shading.

1259
1260
1261
1262
1263
1264
1265
1266
1267
1268



1284 **Fig. A6** Zonally averaged downwelling longwave radiation at the surface (LW_{sfc}^{\downarrow} , in
1285 W/m^2) for (a) the annual mean, (b) December-January-February, and (c) June-July-August
1286 for each continental configuration. Shading indicates $\pm 1\sigma$ of interannual variability.

1287
1288

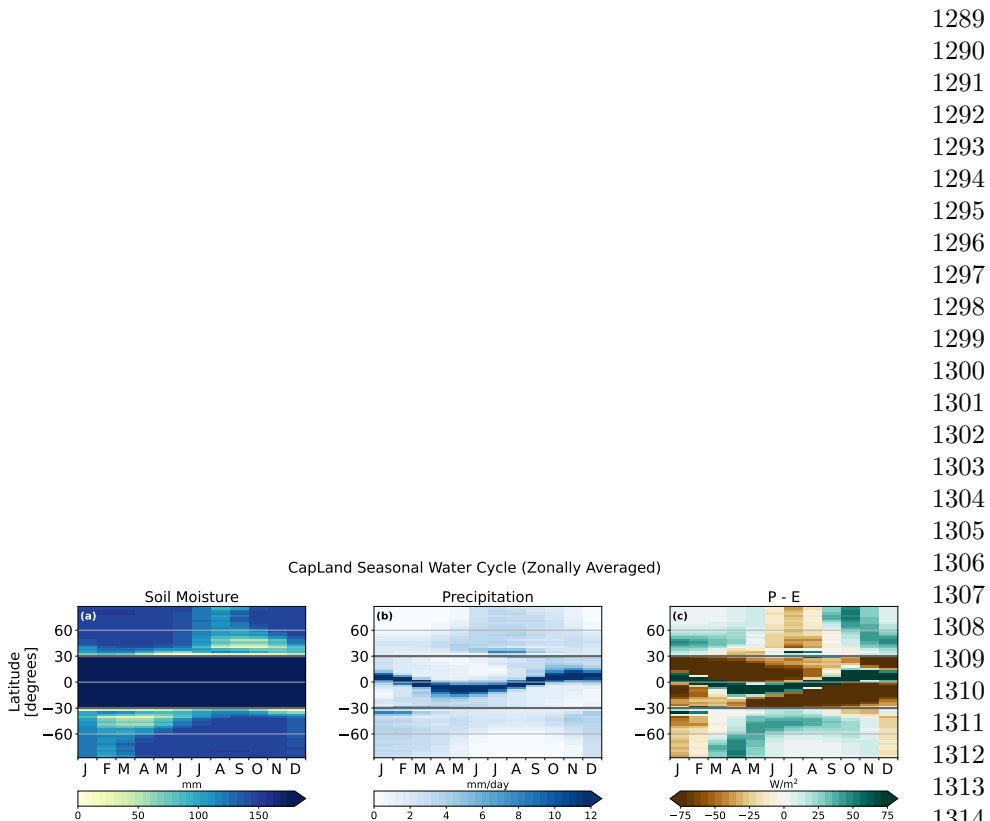


Fig. A7 Zonally averaged (a) soil moisture [mm], (b) precipitation [mm/day], and (c) precipitation-evaporation [W/m^2] over the course of the year for the CapLand simulation. Dark gray lines at 30° N/S indicate the continental/ocean boundary.

1289
1290
1291
1292
1293
1294
1295
1296
1297
1298
1299
1300
1301
1302
1303
1304
1305
1306
1307
1308
1309
1310
1311
1312
1313
1314
1315
1316
1317
1318
1319
1320
1321
1322
1323
1324
1325
1326
1327
1328
1329
1330
1331
1332
1333
1334

30 *Continental configuration controls the base-state water vapor...*

1335 **Declarations**

1336

1337 **Ethical Approval.** Not applicable.

1338

1339

1340

1341

1342

1343

1344 **Competing Interests.** The authors have no relevant financial or non-
1345 financial interests to disclose.

1346

1347

1348

1349

1350

1351

1352 **Author Contributions.** Marysa M. Lagu  designed the study, conducted
1353 the simulations, and conducted the analysis. Marysa M. Lagu  and Sarah
1354 Ragen discussed the preliminary concept of the study. Marysa M. Lagu , Gre-
1355 gory R. Quetin, and William R. Boos discussed results and further analysis.
1356 Sarah Ragen conducted the literature review. The first draft of the manuscript
1357 was written by Marysa M. Lagu  and all authors contributed to and com-
1358 mented on intermediate versions of the manuscript. All authors read and
1359 approved the final manuscript.

1360

1361

1362

1363

1364

1365

1366

1367 **Funding.** M.M.L. acknowledges funding support from the James S. McDon-
1368 nell Foundation Postdoctoral Fellowship in Dynamic and Multiscale Systems.

1369

1370

1371

1372

1373

1374

1375 **Data Availability.** Isca is publicly available on github at <https://github.com/ExeClim/Isca>. The specific version of Isca used in this study is archived
1376 on zenodo and github with the DOI 10.5281/zenodo.6800218. The analysis
1377 code, output from model simulations, python driver scripts, and modifications
1378 to the source code used in this study are publicly archived on zenodo with the
1379 DOI 10.5281/zenodo.7964297 and 10.5281/zenodo.7754428 .

1380

References

- Baldocchi DD, Vogel CA, Hall B (1997) Seasonal variation of energy and water vapor exchange rates above and below a boreal jack pine forest canopy generally less than one-half was wet , daily evaporation. *Journal of Geophysical Research* 102(96):28,928–939,951. <https://doi.org/10.1029/96JD03325> 1381
- Baross JA, Benner SA, Cody GD, et al (2007) The Limits of Organic Life in Planetary Systems. National Academies Press, Washington, DC, <https://doi.org/10.17226/11919> 1382
- Barron EJ, Thompson SL, Hay WW (1984) Continental distribution as a forcing factor for global-scale temperature. *Nature* 310(5978):574–575. <https://doi.org/10.1038/310574a0> 1383
- Barsugli J, Shin SI, Sardeshmukh PD (2005) Tropical climate regimes and global climate sensitivity in a simple setting. *Journal of the Atmospheric Sciences* 62(4):1226–1240. <https://doi.org/10.1175/JAS3404.1> 1384
- Betts AK (1986) A new convective adjustment scheme. Part I: Observational and theoretical basis. *Quarterly Journal of the Royal Meteorological Society* 112(473):677–691. <https://doi.org/10.1002/qj.49711247307> 1385
- 1386
- Betts AK, Miller MJ (1986) A new convective adjustment scheme. Part II: Single column tests using GATE wave, BOMEX, ATEX and arctic air-mass data sets. *Quarterly Journal of the Royal Meteorological Society* 112(473):693–709. <https://doi.org/10.1002/qj.49711247308> 1387
- Bonan GB (2008) Forests and climate change: Forcings, feedbacks, and the climate benefits of forests. *Science (New York, NY)* 320(5882):1444–1449. <https://doi.org/10.1126/science.1155121> 1388
- Budyko MI (1961) The Heat Balance of the Earth's Surface. *Soviet Geography* 2(4):3–13. <https://doi.org/10.1080/00385417.1961.10770761> 1389
- Budyko MI (1969) The effect of solar radiation variations on the climate of the Earth. *Tellus* 21(5):611–619. <https://doi.org/10.3402/tellusa.v21i5.10109> 1390
- Burke CJ, Christiansen JL, Mullally F, et al (2015) TERRESTRIAL PLANET OCCURRENCE RATES for the KEPLER GK DWARF SAMPLE. *Astrophysical Journal* 809(1):8. <https://doi.org/10.1088/0004-637X/809/1/8> 1391
- Cess RD, Goldenberg SD (1981) The effect of ocean heat capacity upon global warming due to increasing atmospheric carbon dioxide. *Journal of Geophysical Research* 86(80):498–502 1392
- 1393
- 1394
- 1395
- 1396
- 1397
- 1398
- 1399
- 1400
- 1401
- 1402
- 1403
- 1404
- 1405
- 1406
- 1407
- 1408
- 1409
- 1410
- 1411
- 1412
- 1413
- 1414
- 1415
- 1416
- 1417
- 1418
- 1419
- 1420
- 1421
- 1422
- 1423
- 1424
- 1425
- 1426

- 1427 Chandler MA, Rind D, Ruedy R (1992) Pangaean climate during the early
1428 Jurassic: GCM simulations and the sedimentary record of paleoclimate. Geo-
1429 logical Society of America Bulletin 104(5):543–559. [https://doi.org/10.1130/0016-7606\(1992\)104<543:PCDTEJ>2.3.CO;2](https://doi.org/10.1130/0016-7606(1992)104<543:PCDTEJ>2.3.CO;2)
- 1431
- 1432 Charney J, Stone PH, Quirk WJ (1975) Drought in Sahara - Biogeophysical
1433 Feedback Mechanism. Science 187(4175):434–435. <https://doi.org/doi:10.1126/science.187.4175.434>
- 1435
- 1436 Chiang JC (2009) The tropics in paleoclimate. Annual Review of Earth
1437 and Planetary Sciences 37:263–297. <https://doi.org/10.1146/annurev.earth.031208.100217>
- 1438
- 1439 Cho MH, Yang AR, Baek EH, et al (2018) Vegetation-cloud feedbacks to future
1440 vegetation changes in the Arctic regions. Climate Dynamics 50(9-10):3745–
1441 3755. <https://doi.org/10.1007/s00382-017-3840-5>
- 1442
- 1443 Clough SA, Shephard MW, Mlawer EJ, et al (2005) Atmospheric radiative
1444 transfer modeling: A summary of the AER codes. Journal of Quantitative
1445 Spectroscopy and Radiative Transfer 91(2):233–244. <https://doi.org/10.1016/j.jqsrt.2004.05.058>
- 1444
- 1445 Cronin TW, Emanuel KA, Molnar P (2015) Island precipitation enhancement
1446 and the diurnal cycle in radiative-convective equilibrium. Quarterly Journal
1447 of the Royal Meteorological Society 141(689):1017–1034. <https://doi.org/10.1002/qj.2443>
- 1448
- 1449 Davin EL, de Noblet-Ducoudré N, de Noblet-Ducoudre N, et al (2010)
1450 Climatic Impact of Global-Scale Deforestation: Radiative versus Nonradiative
1451 Processes. Journal of Climate 23(1):97–112. <https://doi.org/10.1175/2009JCLI3102.1>
- 1452
- 1453 Dirmeyer PA (1998) Land-sea geometry and its effect on monsoon circulations.
1454 Journal of Geophysical Research Atmospheres 103(D10):11,555–11,572.
1455 <https://doi.org/10.1029/98JD00802>
- 1456
- 1457 Donohoe A, Battisti DS (2011) Atmospheric and surface contributions to
1458 planetary albedo. Journal of Climate 24(16):4402–4418. <https://doi.org/10.1175/2011JCLI3946.1>
- 1459
- 1460 Donohoe A, Marshall J, Ferreira D, et al (2013) The relationship between ITCZ
1461 location and cross-equatorial atmospheric heat transport: From the seasonal
1462 cycle to the Last Glacial Maximum. Journal of Climate 26(11):3597–3618.
1463 <https://doi.org/10.1175/JCLI-D-12-00467.1>
- 1464
- 1465 Eliassen A, Palm E (1960) On the Transfer of Energy in Stationary Mountain
1466 Waves. Geofysiske Publikasjoner
1467
- 1468
- 1469
- 1470
- 1471
- 1472

- Enderton D, Marshall J (2009) Explorations of Atmosphere–Ocean–Ice Climates on an Aquaplanet and Their Meridional Energy Transports. *Journal of the Atmospheric Sciences* 66(6):1593–1611. <https://doi.org/10.1175/2008JAS2680.1> 1473
 1474
 1475
 1476
 1477
- Fajber R, Kushner PJ (2021) Using ‘heat tagging’ to understand the remote influence of atmospheric diabatic heating through long-range transport. *Journal of the Atmospheric Sciences* <https://doi.org/10.1175/JAS-D-20-0290.1> 1478
 1479
 1480
 1481
 1482
- Ferrari R, Ferreira D (2011) What processes drive the ocean heat transport? *Ocean Modelling* <https://doi.org/10.1016/j.ocemod.2011.02.013> 1483
 1484
- Ferreira D, Marshall J, Campin JM (2010) Localization of deep water formation: Role of atmospheric moisture transport and geometrical constraints on ocean circulation. *Journal of Climate* 23(6):1456–1476. <https://doi.org/10.1175/2009JCLI3197.1> 1485
 1486
 1487
 1488
 1489
- Frierson DM (2007) The dynamics of idealized convection schemes and their effect on the zonally averaged tropical circulation. *Journal of the Atmospheric Sciences* 64(6):1959–1974. <https://doi.org/10.1175/JAS3935.1> 1490
 1491
 1492
 1493
- Geen R, Lambert FH, Vallis GK (2018) Regime change behavior during Asian monsoon onset. *Journal of Climate* 31(8):3327–3348. <https://doi.org/10.1175/JCLI-D-17-0118.1> 1494
 1495
 1496
 1497
- Harris CR, Millman KJ, van der Walt SJ, et al (2020) Array programming with NumPy. *Nature* 585(7825):357–362. <https://doi.org/10.1038/s41586-020-2649-2> 1498
 1499
 1500
 1501
- Held IM (1985) Pseudomomentum and the orthogonality of modes in shear flows. *Journal of the Atmospheric Sciences* 42(21):2280–2288. [https://doi.org/10.1175/1520-0469\(1985\)042<2280:PATOOM>2.0.CO;2](https://doi.org/10.1175/1520-0469(1985)042<2280:PATOOM>2.0.CO;2) 1502
 1503
 1504
- Held IM, Ting M, Wang H (2002) Northern winter stationary waves: Theory and modeling. *Journal of Climate* 15(16):2125–2144. [https://doi.org/10.1175/1520-0442\(2002\)015<2125:NWSWTA>2.0.CO;2](https://doi.org/10.1175/1520-0442(2002)015<2125:NWSWTA>2.0.CO;2) 1505
 1506
 1507
 1508
- Herman GF, Wu MLC, Johnson WT (1980) The Effect of Clouds on the Earth’s Solar and Infrared Radiation Budgets. *Journal of the Atmospheric Sciences* 37(June):1251–1261 1509
 1510
 1511
 1512
- Hoffman PF, Schrag DP (2002) The snowball Earth hypothesis: Testing the limits of global change. *Terra Nova* 14(3):129–155. <https://doi.org/10.1046/j.1365-3121.2002.00408.x> 1513
 1514
 1515
 1516
 1517
 1518

- 1519 Hoffman PF, Kaufman AJ, Halverson GP, et al (1998) A Neoproterozoic Snow-
1520 ball Earth. *Science* 281(5381):1342–1346. <https://doi.org/10.1126/science.281.5381.1342>
- 1522
- 1523 Hoffman PF, Abbot DS, Ashkenazy Y, et al (2017) Snowball Earth cli-
1524 mate dynamics and Cryogenian geology-geobiology. *Science Advances* 3(11).
1525 <https://doi.org/10.1126/sciadv.1600983>
- 1526
- 1527 Houze RA (2012) Orographic effects on precipitating clouds. *Reviews of
Geophysics* 50(1):1–47. <https://doi.org/10.1029/2011RG000365>
- 1528
- 1529 Hoyer S, Hamman J (2017) Xarray: N-D labeled arrays and datasets in Python.
1530 *Journal of Open Research Software* 5(1). <https://doi.org/10.5334/jors.148>
1531
- 1532 Hu S, Boos WR (2017) The physics of orographic elevated heating in radiative-
1533 convective equilibrium. *Journal of the Atmospheric Sciences* 74(9):2949–
1534 2965. <https://doi.org/10.1175/JAS-D-16-0312.1>
1535
- 1536 Hui KL, Bordoni S (2021) Response of monsoon rainfall to changes in the
1537 latitude of the equatorward coastline of a zonally symmetric continent. *Jour-
1538 nal of the Atmospheric Sciences* 78(5):1429–1444. [https://doi.org/10.1175/JAS-D-20-0110.1](https://doi.org/10.1175/
1539 JAS-D-20-0110.1)
1540
- 1541 IPCC (2013) Climate Change 2013 The Physical Change Basis. Climate
1542 Change 2013: The Physical Science Basis Contribution of Working Group I
1543 to the Fifth Assessment Report of the Intergovernmental Panel on Climate
1544 Change <https://doi.org/10.1017/CBO9781107415324>
1545
- 1546 Jin Z, Charlock TP, Smith WL, et al (2004) A parameterization of ocean
1547 surface albedo. *Geophysical Research Letters* 31(22):1–4. [https://doi.org/10.1029/2004GL021180](https://doi.org/
1548 10.1029/2004GL021180)
- 1549
- 1550 Kang SM, Held IM, Frierson DMW, et al (2008) The Response of the ITCZ
1551 to Extratropical Thermal Forcing: Idealized Slab-Ocean Experiments with
1552 a GCM. *Journal of Climate* 21(14):3521–3532. [https://doi.org/10.1175/2007JCLI2146.1](https://doi.org/10.1175/
1553 2007JCLI2146.1)
- 1554
- 1555 Kang SM, Frierson DMW, Held IM (2009) The Tropical Response to Extrat-
1556ropical Thermal Forcing in an Idealized GCM: The Importance of Radiative
1557 Feedbacks and Convective Parameterization. *Journal of the Atmospheric
1558 Sciences* 66(9):2812–2827. <https://doi.org/10.1175/2009JAS2924.1>
- 1559 Khanna J, Medvigy D (2014) Strong control of surface roughness vari-
1560 ations on the simulated dry season regional atmospheric response to
1561 contemporary deforestation in Rondônia, Brazil. *Journal of Geophysical
1562 Research D: Atmospheres* 119(23):13,067–13,078. [https://doi.org/10.1002/2014JD022278](https://doi.org/10.1002/
1563 2014JD022278)
1564

- Kiehl JT, Trenberth KE (1997) Earth's annual global mean energy budget. *Bulletin of the American meteorological society* 78(2):197–208 1565
1566
1567
- Kim JE, Laguë MM, Pennypacker S, et al (2020) Evaporative Resistance is of Equal Importance as Surface Albedo in High-Latitude Surface Temperatures Due to Cloud Feedbacks. *Geophysical Research Letters* 47(4). <https://doi.org/10.1029/2019GL085663> 1568
1569
1570
1571
1572
- Kirshbaum DJ, Smith RB (2009) Orographic precipitation in the tropics: Large-Eddy simulations and theory. *Journal of the Atmospheric Sciences* 66(9):2559–2578. <https://doi.org/10.1175/2009JAS2990.1> 1573
1574
1575
- Kirtman BP, Shukla J (2000) Influence of the Indian summer monsoon on ENSO. *Quarterly Journal of the Royal Meteorological Society* 126(562):213–239. <https://doi.org/10.1002/qj.49712656211> 1576
1577
1578
1579
- Kite ES, Ford EB (2018) Habitability of Exoplanet Waterworlds. *The Astrophysical Journal* 864(1):75. <https://doi.org/10.3847/1538-4357/aad6e0> 1580
1581
1582
- Knippertz P, Wernli H (2010) A Lagrangian Climatology of Tropical Moisture Exports to the Northern Hemispheric Extratropics. *Journal of Climate* 23(4):987–1003. <https://doi.org/10.1175/2009JCLI3333.1> 1583
1584
1585
1586
- Kooperman GJ, Chen Y, Hoffman FM, et al (2017) Forest response to rising CO₂ drives zonally asymmetric rainfall change over tropical continents. *Nature Climate Change* 8(5):1–36. <https://doi.org/10.1038/s41558-018-0144-7> 1587
1588
1589
1590
- Kottek M, Grieser J, Beck C, et al (2006) World map of the Köppen-Geiger climate classification updated. *Meteorologische Zeitschrift* 15(3):259–263. <https://doi.org/10.1127/0941-2948/2006/0130> 1591
1592
1593
1594
- Laguë MM, Bonan GB, Swann ALS (2019) Separating the Impact of Individual Land Surface Properties on the Terrestrial Surface Energy Budget in both the Coupled and Uncoupled Land–Atmosphere System. *Journal of Climate* 32(18):5725–5744. <https://doi.org/10.1175/jcli-d-18-0812.1> 1595
1596
1597
1598
1599
- Laguë MM, Pietschnig M, Ragen S, et al (2021) Terrestrial evaporation and global climate: Lessons from Northland, a planet with a hemispheric continent. *Journal of Climate* 34(6):2253–2276. <https://doi.org/10.1175/jcli-d-20-0452.1> 1600
1601
1602
1603
1604
- Loft G (1918) The Gulf Stream and the North Atlantic Drift. *Journal of Geography* 17(1):8–17. <https://doi.org/10.1080/00221341808984367> 1605
1606
1607
- Macdonald FA, Swanson-hysell NL, Park Y, et al (2019) Arc-continent collisions in the tropics set Earth's climate state. *Science* 184(April):181–184 1608
1609
1610

- 1611 Manabe S, Terpstra TB (1974) The effect of moutains on the general
1612 circulation of the Atmosphere. *Journal of the Atmospheric Sciences* 31(1):3
1613
- 1614 Manabe SYUKURO (1969) Climate and the Ocean Circulation. *Monthly
1615 Weather Review* 97(11):739–774. [https://doi.org/10.1175/1520-0493\(1969\)
097\(0739:CATOC\)2.3.CO;2](https://doi.org/10.1175/1520-0493(1969)
097(0739:CATOC)2.3.CO;2)
- 1617 Maroon EA, Frierson DM (2016) The impact of a continent's longi-
1618 tudinal extent on tropical precipitation. *Geophysical Research Letters*
1619 43(22):11,921–11,929. <https://doi.org/10.1002/2016GL071518>
- 1621 Maroon EA, Frierson DM, Battisti DS (2015) The tropical precipita-
1622 tion response to Andes topography and ocean heat fluxes in an aqua-
1623 planet model. *Journal of Climate* 28(1):381–398. [https://doi.org/10.1175/
JCLI-D-14-00188.1](https://doi.org/10.1175/
1624 JCLI-D-14-00188.1)
- 1626 McFarlane NA (1987) The Effect of Orographically Excited Gravity Wave
1627 Drag on the General Circulation of the Lower Stratosphere and Troposphere.
1628 *Journal of the Atmospheric Sciences* 44(14):1775–1800. [https://doi.org/10.
1675/1520-0469\(1987\)044\(1775:teooeg\)2.0.co;2](https://doi.org/10.
1675/1520-0469(1987)044(1775:teooeg)2.0.co;2)
- 1630
- 1631 Méndez A, Rivera-Valentín EG, Schulze-Makuch D, et al (2021) Habitability
1632 Models for Astrobiology. *Astrobiology* 21(8):1017–1027. [https://doi.org/10.
1089/ast.2020.2342](https://doi.org/10.
1089/ast.2020.2342)
- 1634
- 1635 Meredith AS, Williams SE, Collins AS, et al (2021) Extending full-plate
1636 tectonic models into deep time: Linking the Neoproterozoic and the Phanero-
1637 zoic. *Earth-Science Reviews* 214(December 2020):103,477. [https://doi.org/
10.1016/j.earscirev.2020.103477](https://doi.org/
1638 10.1016/j.earscirev.2020.103477)
- 1639
- 1640 Mlawer EJ, Taubman SJ, Brown PD, et al (1997) Radiative transfer for inho-
1641 mogeneous atmospheres: RRTM, a validated correlated-k model for the
1642 longwave. *Journal of Geophysical Research: Atmospheres* 102(D14):16,663–
1643 16,682. <https://doi.org/10.1029/97JD00237>
- 1644
- 1645 North GR, Mengel JG, Short DA (1983) Simple energy balance model resolving
1646 the seasons and the continents: Application to the astronomical theory of
1647 the ice ages. *Journal of Geophysical Research* 88(C11):6576–6586. [//doi.org/10.1029/JC088iC11p06576](https:
1648 //doi.org/10.1029/JC088iC11p06576)
- 1649 Payne RE (1972) Albedo of the Sea Surface. *Journal of the Atmospheric
1650 Sciences* 29(5):959–970. [https://doi.org/10.1175/1520-0469\(1972\)029<0959:
aotss>2.0.co;2](https://doi.org/10.1175/1520-0469(1972)029<0959:
1651 aotss>2.0.co;2)
- 1653 Penn JL, Deutsch C, Payne JL, et al (2018) Temperature-dependent hypoxia
1654 explains biogeography and severity of end-Permian marine mass extinction.
1655 *Science* 362(6419). <https://doi.org/10.1126/science.aat1327>
- 1656

Pierrehumbert RT (2010) Principles of Planetary Climate, 1st edn. Cambridge University Press, https://doi.org/10.1017/CBO9780511780783	1657 1658 1659
Pietschnig M, Swann AL, Lambert FH, et al (2021) Response of tropical rainfall to reduced evapotranspiration depends on continental extent. <i>Journal of Climate</i> 34(23):9221–9234. https://doi.org/10.1175/JCLI-D-21-0195.1	1660 1661 1662
Queney P (1948) The Problem of Air Flow Over Mountains: A Summary of Theoretical Studies. <i>Bulletin of the American Meteorological Society</i> 29(1):16–26. https://doi.org/10.1175/1520-0477-29.1.16	1663 1664 1665 1666
Richardson PL (1980) Benjamin Franklin and Timothy Folger's First Printed Chart of the Gulf Stream. <i>Science</i> 207(4431):643–645	1667 1668 1669
Rushby AJ, Shields AL, Wolf ET, et al (2020) The Effect of Land Albedo on the Climate of Land-dominated Planets in the TRAPPIST-1 System. <i>The Astrophysical Journal</i> 904(2):124. https://doi.org/10.3847/1538-4357/abbe04	1670 1671 1672 1673 1674
Salem BBC (1989) Arid zone forestry: A guide for field technicians. FAO Conservation Guide No. 20	1675 1676 1677
Saulière J, Brayshaw DJ, Hoskins B, et al (2012) Further Investigation of the Impact of Idealized Continents and SST Distributions on the Northern Hemisphere Storm Tracks. <i>Journal of the Atmospheric Sciences</i> 69(3):840–856. https://doi.org/10.1175/JAS-D-11-0113.1	1678 1679 1680 1681
Seager S (2013) Exoplanet Habitability. <i>The Astrophysical Journal</i> 340(May):577–582. https://doi.org/10.1088/0004-637X/777/2/95	1682 1683 1684
Shukla J, Mintz Y (1982) Influence of Land-Surface Evapotranspiration on the Earth's Climate. <i>Science</i> 215(4539):1498–1501. https://doi.org/10.1126/science.215.4539.1498	1685 1686 1687 1688
Sikma M, Vilà-Guerau de Arellano J (2019) Substantial Reductions in Cloud Cover and Moisture Transport by Dynamic Plant Responses. <i>Geophysical Research Letters</i> 46(3):1870–1878. https://doi.org/10.1029/2018GL081236	1689 1690 1691 1692
Stefan J (1879) On the relationship between thermal radiation and temperature. <i>Bulletin from the sessions of the Vienna Academy of Sciences (Vienna, 1879)</i> 79:391–428	1693 1694 1695 1696
Stone PH (1978) Baroclinic Adjustment. <i>Journal of the Atmospheric Sciences</i> 35(April):561–571	1697 1698 1699
Straume EO, Gaina C, Medvedev S, et al (2020) Global Cenozoic Paleobathymetry with a focus on the Northern Hemisphere Oceanic Gateways.	1700 1701 1702

- 1703 Gondwana Research 86:126–143. <https://doi.org/10.1016/j.gr.2020.05.011>
1704
- 1705 Sud YC, Shukla J, Mintz Y (1988) Influence of Land Surface Roughness on
1706 Atmospheric Circulation and Precipitation: A Sensitivity Study with a Gen-
1707 eral Circulation Model. Journal of Applied Meteorology 27(9):1036–1054.
1708 [https://doi.org/10.1175/1520-0450\(1988\)027<1036:iolsro>2.0.co;2](https://doi.org/10.1175/1520-0450(1988)027<1036:iolsro>2.0.co;2)
- 1709
- 1710 Thomson SI, Vallis GK (2019) Hierarchical modeling of solar sys-
1711 tem planets with Isca. Atmosphere 10(12):1–21. <https://doi.org/10.3390/ATMOS10120803>
- 1712
- 1713 Tierney JE, Poulsen CJ, Montañez IP, et al (2020) Past climates inform
1714 our future. Science 370(6517):eaay3701. <https://doi.org/10.1126/science.aay3701>
- 1715
- 1716
- 1717 Vallis GK, Colyer G, Geen R, et al (2018) Isca, v1.0: A framework for the
1718 global modelling of the atmospheres of Earth and other planets at varying
1719 levels of complexity. Geoscientific Model Development 11(3):843–859. <https://doi.org/10.5194/gmd-11-843-2018>
- 1721
- 1722 Van Rossum G, Drake FL (2009) Python 3 Reference Manual. CreateSpace,
1723 Scotts Valley, CA, <https://doi.org/10.5555/1593511>
- 1724
- 1725 Virtanen P, Gommers R, Oliphant TE, et al (2020) SciPy 1.0: Fundamental
1726 algorithms for scientific computing in Python. Nature Methods 17(3):261–
1727 272. <https://doi.org/10.1038/s41592-019-0686-2>
- 1728
- 1729 Voigt A (2013) The dynamics of the Snowball Earth Hadley circulation for
1730 off-equatorial and seasonally varying insolation. Earth System Dynamics
1731 4(2):425–438. <https://doi.org/10.5194/esd-4-425-2013>
- 1732
- 1733 Voigt A, Held IM, Marotzke J (2012) Hadley cell dynamics in a virtually dry
1734 snowball Earth atmosphere. Journal of the Atmospheric Sciences 69(1):116–
1735 128. <https://doi.org/10.1175/JAS-D-11-083.1>
- 1736
- 1737 Voigt A, Bony S, Dufresne JL, et al (2014) The radiative impact of clouds
1738 on the shift of the Intertropical Convergence Zone. Geophysical Research
1739 Letters 41(12):4308–4315. <https://doi.org/10.1002/2014GL060354>
- 1740
- 1741 Voosen P (2019) A 500-million-year survey of Earth's climate reveals dire
1742 warning for humanity. Science <https://doi.org/10.1126/science.aay1323>
- 1742
- 1743 White RH, Battisti DS, Roe GH (2017) Mongolian mountains matter most:
1744 Impacts of the latitude and height of asian orography on pacific wintertime
1745 atmospheric circulation. Journal of Climate 30(11):4065–4082. <https://doi.org/10.1175/JCLI-D-16-0401.1>
- 1747
- 1748

Continental configuration controls the base-state water vapor... 39

Wiscombe W, Warren S (1980) A Model for Spectral Albedo I: Pure Snow	1749
	1750
Worsley TR, Kidder DL (1991) First-order coupling of paleogeography and CO ₂ , with global surface temperature and its latitudinal contrast. Geology 19(12):1161–1164. <a href="https://doi.org/10.1130/0091-7613(1991)019<1161:FOCOPA>2.3.CO;2">https://doi.org/10.1130/0091-7613(1991)019<1161:FOCOPA>2.3.CO;2	1751
	1752
	1753
	1754
	1755
Yasunari T, Saito K, Takata K (2006) Relative roles of large-scale orography and land surface processes in the global hydroclimate. Part I: Impacts on monsoon systems and the tropics. Journal of Hydrometeorology 7(4):626–641. https://doi.org/10.1175/JHM515.1	1756
	1757
	1758
	1759
Zelinka MD, Randall DA, Webb MJ, et al (2017) Clearing clouds of uncertainty. Nature Climate Change 7(10):674–678. https://doi.org/10.1038/nclimate3402	1760
	1761
	1762
	1763
Zhai J, Boos WR (2017) The drying tendency of shallow meridional circulations in monsoons. Quarterly Journal of the Royal Meteorological Society 143(708):2655–2664. https://doi.org/10.1002/qj.3091	1764
	1765
	1766
	1767
Zhou W, Xie SP (2018) A hierarchy of idealized monsoons in an intermediate GCM. Journal of Climate 31(22):9021–9036. https://doi.org/10.1175/JCLI-D-18-0084.1	1768
	1769
	1770
	1771
	1772
	1773
	1774
	1775
	1776
	1777
	1778
	1779
	1780
	1781
	1782
	1783
	1784
	1785
	1786
	1787
	1788
	1789
	1790
	1791
	1792
	1793
	1794